1 2  9 0

UNIVERSIDADE D
COIMBRA

Joana Machado Sampaio

CEREBRAL REORGANIZATION AND NEUROSENSORY PLASTICITY

Dissertation submitted to the Department of Physics
of the Faculty of Science and Technology of the University of Coimbra
in partial fulfillment of the requirements
for the Degree of Master in Biomedical Engineering

July de 2019

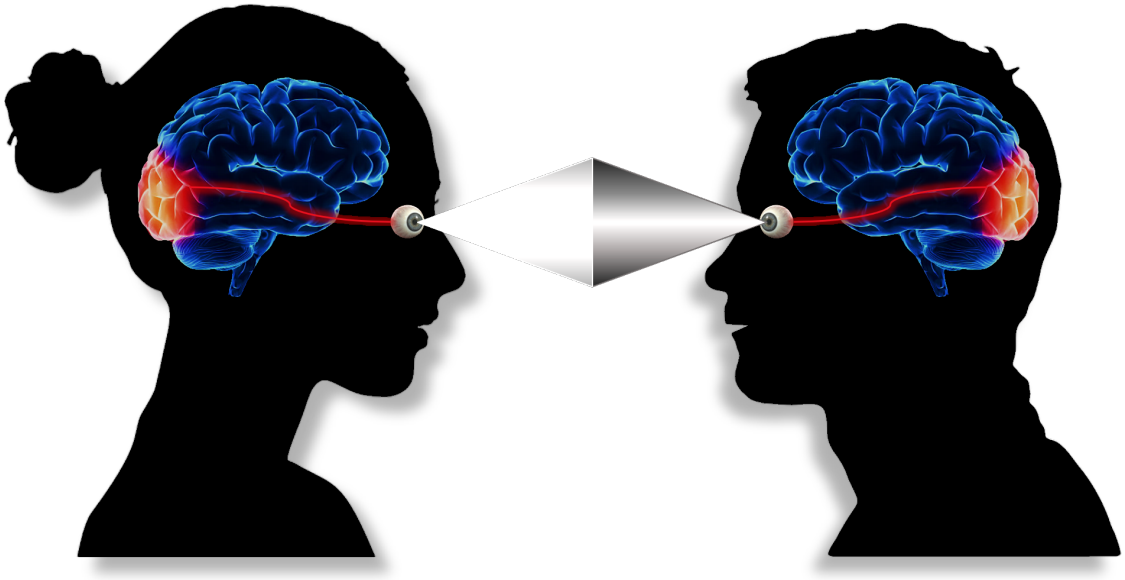

JOANA MACHADO SAMPAIO

CEREBRAL REORGANIZATION AND NEUROSENSORY PLASTICITY

Thesis submitted to the University of Coimbra

for the degree of Master in Biomedical Engineering

Supervisors:

Prof. Dra. Otília C. D'Almeida

Prof. Dr. Miguel Castelo Branco

Faculty of Medicine, University of Coimbra, Coimbra, Portugal;

CiBIT, Institute for Nuclear Sciences Applied to Health (ICNAS), University of Coimbra, Coimbra, Portugal

Coimbra, 2019

This work was developed in collaboration with:

ICNAS

Faculty of Sciences and Technology of the University of Coimbra

CIBIT

Dedication

Um obrigado à minha orientadora Otília d'Almeida e ao professor Miguel Castelo-Branco por tudo o apoio e ajuda ao longo destes meses. Agradeço especialmente à Otília por tão amavelmente ter partilhado o seu gabinete comigo e à Ana por todas as vezes que me abriu a porta.

Agradeço aos meus pais Helena e Carlos por todo esforço que fizeram para eu cá estar, por acreditarem em mim e por todo o apoio moral que me deram para eu não desanimar. Ao meu irmão David por confiar em mim desde o início e nunca me deixar pendurada quando ia a casa, mesmo quando lhe apetecia. À Cris, *my person*, por estar sempre lá, mesmo estando longe, para ouvir todas as minhas dúvidas existenciais nas fases de crise, por nunca ter desistido de mim e, especialmente, por me levar a comer a sítios muito bons em todos os momentos de descontração. Ao Gustavo, *my Boo*, pelos jantares à pala, pelas músicas para relaxar e para trabalhar melhor, e por me fazer rir mesmo quando estou cansada e sem paciência. À Maria, por todas as noitadas a trabalhar sempre de bom humor e com imensa comida e música à mistura, e por me fazer acreditar que eu conseguia. Ao Osh e à Maggie por todo o apoio e amor à distância que só eles sabem dar. À Anocas agradeço por ser super fofa e me encorajar a trabalhar com uma ida ao sushi.

Descobri que o segredo para a realização de uma tese não é só trabalhar arduamente. Nada disto seria possível sem uma família excelente, amigos incríveis e boa comida à mistura.

Acknowledgments

This work was supported by the Portuguese Funding Agency for Science and Technology (FCT) grants E-Rare2-SAU/0001/2008, E-Rare4/0001/2012, COMPETE, POCI-01-0145-FEDER-007440, FCT. UID/NEU/04539/2013–2020, MEDPERSYST, POCI-01-0145-FEDER-016428, and BIGDATIMAGE, CENTRO-01-0145-FEDER-000016 financed by Centro 2020 FEDER, COMPETE.

Author Contribution

This thesis is a follow-up work of Sónia Ferreira [1]. The author of this thesis, Joana Sampaio, participated in every step of MRI data processing, analysis of the results and the writing of the present report.

“Use your smile to change the world;

don’t let the world change your smile.”

Chinese Proverb

Aos 5 anos. À paciência. Sobretudo, às boas memórias.

Abstract

The topic of neural plasticity is very contemporary but is still very controversial. Plasticity reflects changes on the structure and function following environmental demands throughout life. The visual system is one of the finest models to study plasticity phenomena due to the extensive knowledge of its structure and properties.

Indeed, there is a lack of human studies investigating the alterations caused by a loss of input from peripheral vision. In this work we questioned if populations of visual neurons do reorganize in response to a genetically-determined perceptual alteration due to peripheral loss of vision (scotomas) in adults. Retinitis Pigmentosa (RP) is a rare disease that leads to the degeneration of photoreceptors causing a loss of the peripheral visual field that progresses towards the center.

We acquired anatomical and functional data from twelve patients in different stages of the disease and twenty-five healthy controls in order to study population receptive field (pRF) properties of visual neurons, whose alterations can be indicative of reorganization in response to the loss of sensory input. We used a recent technique called population receptive field (pRF) mapping, an optimized alternative to traditional Retinotopy, to estimate the sizes of population receptive fields for each hemisphere of each participant.

In general, mean pRF sizes showed the expected increase within the visual areas along 11 degrees of eccentricity. However, the pattern of the variation was different from controls. Moreover, the analysis of slopes of the fitting lines for each visual area and between RP and Control groups revealed a significant interaction. In fact, in contrast to controls, the degree of change of mean pRF sizes along eccentricity was similar across visual areas in RP, suggesting a loss of input convergence from V1 to V2, and later to V3. Furthermore,

the mean pRF size of V1 in the peripheral representations was significantly higher in RP patients, which indicates a functional reorganization to compensate the lack of peripheral visual input. In order to understand if this remapping is a short-term adaptation or a long-term plasticity phenomena, we acquired data from controls stimulated with artificial scotomas (AS) simulating the visual field of each RP patient. We found a lower explained variance and lower pRF sizes in the AS group, as compared to RP, confirming that there is long-term plasticity rather than rapid adaptation mechanisms in the latter.

To sum up, we found evidence for long-term reorganization mechanisms of neural pRFs in response to peripheral visual field degeneration in adult RP patients. Therefore, these plasticity phenomena should be taken in consideration due to their strong implications for therapeutic and rehabilitation strategies in these patients.

Resumo

Plasticidade neuronal é um tópico muito contemporâneo mas ao mesmo tempo bastante controverso. O conceito de plasticidade reflete mudanças na estrutura e função por adaptação ao ambiente onde se está inserido ao longo da vida. O sistema visual é um dos modelos mais robustos para estudar fenómenos de plasticidade devido ao vasto conhecimento sobre a sua estrutura e propriedades.

De facto, estudos em humanos investigando as alterações causadas pela falta de informação vinda da visão periférica escasseiam na literatura. Neste trabalho questionamos se populações de neurónios visuais se reorganizam em resposta a alterações percetuais numa doença em que a perda visual é geneticamente pré-determinada resultando em *escotomas* (regiões cegas) periféricos em adultos. A Doença Pigmentar (RP) é uma doença genética rara que leva à degeneração dos fotorrecetores e consequentemente à perda de campo visual periférico, afetando progressivamente a visão central também.

Foram adquiridos dados anatómicos e funcionais de doze doentes em diferentes estágios da doença e vinte-e-cinco indivíduos controlo saudáveis de modo a investigar as propriedades de uma população de campos recetivos (pRF) de neurónios visuais, cujas alterações podem sugerir reorganização em resposta à ausência de informação sensorial. Aplicou-se uma técnica recente denominada mapeamento de *population receptive fields* (pRFs), uma alternativa mais sofisticada à Retinotopia tradicional, de modo a analisar o tamanho dos campos recetores para cada hemisfério de cada participante.

Em geral, e como esperado, os tamanhos médios dos pRFs aumentaram dentro das áreas visuais e ao longo de 11 graus de excentricidade. No entanto, o padrão de variação foi diferente do dos controlos. Além disso, a análise dos declives das retas de ajuste para

cada uma das áreas visuais e entre os grupos RP e Controlo revelou uma interação significativa. Na realidade, ao contrário dos controlos, o grau de mudança dos tamanhos médios dos pRFs ao longo da excentricidade é muito similar nas diferentes áreas visuais de RP, o que sugere uma perda de convergência de informação de V1 para V2, e mais tarde para V3. Em adição, o tamanho médio dos pRFs em V1 na zona de representações periféricas foi significativamente maior nos pacientes com RP, o que indica uma reorganização funcional para compensar a falta de informação recebida por parte da periferia. De forma a clarificar se este remapeamento tem como origem uma adaptação a curto-prazo ou se é devido a fenómenos de plasticidade a longo-prazo, foram adquiridos dados de controlos estimulados com escotomas artificiais (AS) que simulam o campo visual de cada um dos pacientes com RP. Foi verificada uma baixa variância explicada e uma diminuição do tamanho dos pRFs no grupo AS, ao contrário dos doentes, confirmando a existência de plasticidade a longo-prazo em vez de mecanismos de adaptação rápida.

Resumindo, descobrimos evidências de mecanismos de reorganização a longo-prazo na população de campos recetores de neurónios em resposta à degeneração do campo visual periférico em pacientes adultos com RP. Deste modo, estes acontecimentos devem ser levados em consideração devido às suas implicações no desenvolvimento de estratégicas de terapêutica e reabilitação nestes pacientes.

List of acronyms

AC Anterior Commissure

ANOVA Analysis of Variance

AS Artificial Scotoma

BOLD Blood oxygenation level-dependent

CNTR Control

Ecc Eccentricity

FA Flip Angle

fMRI Functional Magnetic Resonance Imaging

FoV Field of View

LPZ Lesion Projection Zone

MD Macular Degeneration

MRI Magnetic Resonance Imaging

MPRAGE Magnetization-Prepared Rapid Acquisition with Gradient Echosequences

PA Polar Angle

PC Posterior Commissure

pRF Population receptive field

PRL Preferred retinal lesion

PTC Predicted time courses

RF Receptive Field

ROI Region-of-interest

RGC Retinal ganglion cells

RP Retinitis Pigmentosa

SNR Signal-to-noise-ratio

STC stimulus time courses

TAL Talairach

TE Echo time

TI Interslice time

TR Repetition time

VA Visual acuity

va Visual angle

VMR Volumetric Magnetic Resonance

List of Figures

1.1 Representation scheme of the eye structure (left) and cellular organization of the retina (right). 3

1.2 Retinocortical Pathway. 4

1.3 Simulation of the visual field perception of a person with RP (A) and a person with normal vision (B). 8

1.4 Different types of stimuli: moving (A) wedge, (B) ring and (C) bar. . . . 10

2.1 Individual static perimetry sensitivity maps of the Retinitis Pigmentosa (RP) patients (1-12). These static visual fields were used as masks for the participants of the artificial scotoma experiment. 15

2.2 To study cortical visual maps, two retinotopic fMRI paradigms were used, comprising (A) a wedge rotating counter-clockwise and (B) an expanding ring stimuli, mapping polar angle positions and eccentricity positions regarding the center of the gaze, respectively. 17

2.3 Illustration of a full cycle of wedge stimuli (*original* Polar Angle stimuli) for RP patients and controls. 18

2.4 Illustration of a complete cycle of ring stimuli (*original* Eccentricity stimuli) for RP patients and controls. 19

2.5 Illustration of a full cycle of wedge stimuli (Polar Angle) for an artificial scotoma participant (AS10). 20

2.6 Illustration of a complete cycle of ring (Eccentricity) stimuli for a artificial scotoma participant (AS10). 21

2.7 Illustration of the anatomical reconstruction steps. 23

3.1 Illustration of the obtained maps that characterize the population receptive fields in terms of (upper row) **size**, (middle row) **eccentricity** and (bottom row) **polar angle** of a control (CNTR4), a patient with RP (RP4) and an artificial scotoma control (AS4). Maps are presented in a pseudo-colour code: **size** varies between 0 (red) and 7 (light blue) degrees of visual angle; **eccentricity** ranges from 0 (red) to 11.5 (dark blue) degrees of visual angle; **polar angle** can alter from -3.14 (dark blue) to 3.14 (dark blue) radians. Both hemispheres are represented. 28

3.2 Representation of the definition of the borders between visual areas on the (A) right hemisphere and (B) the left hemisphere using Polar Angle maps. 29

3.3 Representation of the mean pRF size (degrees) within each eccentricity degree (step: 1º) for each visual area (mean of both hemispheres), V1 (red), V2 (green), V3 (blue) for the RP group. For each visual area a linear fit procedure was performed. Error bars denote standard error of the mean (SEM). 30

3.4 Representation of the mean pRF size (degrees) within each eccentricity degree (step: 1º) for each visual area (mean of both hemispheres), V1 (red), V2 (green), V3 (blue) for the Control group. For each visual area a linear fit procedure was performed. Error bars denote the SEM. 30

3.5 Plot of the estimated marginal means of the slope values of the regression lines of the visual areas V1, V2 and V3 (fitting of the mean pRF sizes along eccentricity bins) in the RP (red circles) and control (blue diamonds) groups. 31

3.6 Plot of the estimated marginal means of the intercept values (β_0) of the regression lines of the visual areas V1, V2 and V3 V3 (fitting of the mean pRF sizes along eccentricity bins) in the RP (red circles) and control (blue diamonds) groups. 32

3.7 Representation of the mean pRF size (degrees) in the peripheral representation of V1 for both RP and control groups. The RP group had higher pRF sizes in the peripheral representations of V1 when compared to the Control group. Error bars denote the SEM. **$p < 0.05$. 33

3.8 Mean pRF size (deg) in the peripheral representation on V1 for the Control group, the RP subgroup with a visual angle (va) greater than 15deg of diameter (RP, va>15deg) and the RP subgroup with va lower or equal to 15deg (RP, va $\leqslant$ 15deg). Error bars denote the SEM. **$p < 0.05$. 34

3.9 Mean pRF size in each eccentricity zone (central, Middle or Periphery) of the visual areas V1 (green), V2 (blue) and V3 (pink) of the RP Group. Error bars denote the SEM. 35

3.10 Mean pRF size in each eccentricity zone (central, Middle or Periphery) of the visual areas V1 (green), V2 (blue) and V3 (pink) of the Control Group. Error bars denote the SEM. 36

3.11 Estimated marginal means of pRF size in V1 between RP (red circles) and Control (blue diamonds) groups and within Central, Middle and Periphery zones. 37

3.12 Estimated marginal means of pRF size in V2 between RP (red circles) and Control (blue diamonds) groups and within Central, Middle and Periphery zones. 37

3.13 Estimated marginal means of pRF size in V3 between RP (red circles) and Control (blue diamonds) groups and within Central, Middle and Periphery zones. 38

3.14 Representation of the mean explained variance R^2 for each eccentricity bin in the occipital lobe region for each group, RP (red), Control (green), Artificial Scotoma (blue). These results correspond to the mean of both hemispheres. The dots represent the mean R^2 value and the shadowed are the associated SEM. 40

3.15 Representation of the mean variance R^2 for each eccentricity bin in the occipital lobe for each group, RP (red), Control (green), Artificial Scotoma (blue). RP8, RP9, AS8 and AS9 were removed from the analysis. These results correspond to the mean of both hemispheres. The dots represent the mean R^2 value and the shadowed area the associated SEM. 41

3.16 Representation of the mean variance R^2 for each eccentricity bin in the occipital lobe, for each group/subgoups, RP (RP, va⩽15deg, red and RP, va>15deg, pink), Control (green), Artificial Scotoma (AS, va⩽15deg dark blue and AS, va>15deg, light blue). These results corresponds to the mean of both hemispheres. The dots represent the mean R^2 value and the shadowed area the associated SEM. 42

3.17 Manual delineation of the calcarine sulcus region (shadow in green) and the deepest part of it (represented as the brown line) on the left hemisphere. 43

3.18 Representation of the mean explained variance R^2 for each eccentricity bin along the calcarine sulcus for each group, RP (red), Control (green), Artificial Scotoma (blue). These results correspond to the mean of both hemispheres. The dots represent the mean R^2 value and the shadowed area the associated SEM. 43

3.19 Representation of the mean explained variance R^2 for each eccentricity bin along the calcarine sulcus for each group, RP (red), Control (green), Artificial Scotoma (blue). These results correspond to the mean of both hemispheres. The dots represent the mean R^2 value and the shadowed area the associated SEM. 44

3.20 Illustration of the mean size of the whole calcarine sulcus for each group, along with the respective standard error. The outcome is the mean of both hemispheres. 44

4.1 Representative model of convergence in the visual system of primates. LGN - lateral geniculate nucleus; V1 - primary visual area; TEO - posterior inferior temporal cortex; TE - inferior temporal cortex. 48

6.1 Data representation of the mean population receptive field sizes in function of eccentricity within visual areas V1, V2 and V3 of all the participants from (A) the control group and (B) the RP group. (C) and (D) represent the same analysis but for RP subgroup with visual angle (va) smaller or equal to 15 degrees (*RP, va* $\leqslant 15$ *deg*) and RP subgroup whose patients had visual angles superior to 15 degrees (*RP, va*> 15 *deg*), respectively. . 67

List of Tables

2.1 Clinico-demographic and ophthalmological characterization of the subjects cohort. Visual acuity was determined using a decimal chart. The extent of visual diameter was based on the static perimetry results by excluding absolute regions (black regions with sensitivity below 10dB). . . 14

6.1 Neuro-ophtalmologic characteristics of the participants' sample. Average Retinal and Retinal Nerve Fiber Layer (RNFL) thickness were measured using frequency domain Cirrus Ocular Coherence Tomography (OCT, software version 5.1.1.6, Carl Zeiss Meditec AG, USA). Moreover, it was used a suprathreshold strategy for the 79 visual field points tested in central 24 deg, or 12 deg when patients had a small visual field, to automatically obtain the visual field deficit volume based on sensitivity values of those points and tested visual area. 65

Contents

List of Figures **xxiii**

List of Tables **xxvii**

1 Introduction **1**

1.1 The concept of neuroplasticity 1

1.2 The basics of the organization of the Visual System 2

1.3 Neuronal visual plasticity 4

1.4 A disease model of peripheral Visual Field degeneration: Retinitis Pigmentosa 7

1.5 Retinotopy and Population Receptive Fields 9

2 Material and Methods **13**

2.1 Participants 13

2.2 Magnetic Resonance Imaging 16

2.3 Stimuli and Experimental Design 16

2.4 Data Analysis 22

2.4.1 Anatomical Processing 22

2.4.2 Functional Processing 23

2.4.3 Population Receptive Fields 24

2.4.4 Statistical Analysis 24

3 Results **27**

3.1 Analysis of the participants sample 27

3.2 Population Receptive Fields Analysis 28

3.2.1 Difference in the patterns of pRF size along eccentricity and visual areas suggest loss of convergence in RP 29
3.2.2 pRF size is higher in peripheral representations of V1 in patients suggesting compensatory mechanisms 33
3.3 Artificial Scotoma in controls do not reflect RP functional maps, indicating reorganization instead of adaptive processes 38
3.3.1 Analysis of Explained Variance along the occipital lobe 39
3.3.2 Analysis of Explained Variance along the calcarine sulcus 42

4 Discussion **47**

5 Conclusion **51**

6 Future Work **53**

Bibliography **55**

Appendices **63**

1

Introduction

1.1 The concept of neuroplasticity

Neuronal plasticity is referred to as the brain capacity to change its structural or functional properties in response to environmental demands [1]. Hence, it excludes innate mechanisms that occur during the early development [2].

Functional plasticity refers to the brain's ability to reorganize its neural activity, by reorienting it to undamaged or functionally active areas, whereas following learning experience, training or brain damage. Structural plasticity involves morphological changes of grey and white matter, for example, an increase in structural connectivity or their volume [3], mainly as a result of learning processes [4].

Distinguishing between the concept of **plasticity** and others like **reorganization** or **adaptation** or even **perceptual learning** is of utmost importance, but the literature is not always consistent. When it comes to the concept of **reorganization**, Ferreira et at. (2017) refers to it as a synonym of plasticity [1] and distinguish these terms from "remapping", which might reflect short-term mechanisms and not necessarily reorganization. Accordingly, Lemos et al. (2016) considers that reorganization must reflect long-term plastic structural changes and warns that some authors also extend the concept to long-term functional changes [5]. **Adaptation**, on the other hand, is often coined as a term to denote short-term functional modifications of neural interactions (Lemos et al. (2016)), in agreement to Wandell et al. (2009) who denotes adaptation as a short-term adjustment often created in response to fluctuations in the dynamic range of inputs or outputs [6]. The synapse

represents the potential for **learning** and **plasticity**, which is considered to reflect a more permanent neuronal modification following changed experience with impact on behaviour [7].

Plasticity can either have a positive (adaptive) or negative (maladaptive) outcome. Adaptive plastic changes entail the reorganization outcome that best fits the demands from the environment. On the other hand, maladaptive changes happen when the result of the reorganization is highly dysfunctional since the brain miswired as a response to the signals from the environment. As an example, it may lead to excessive alterations and even a simple structural may cause significant deleterious effects [2].

1.2 The basics of the organization of the Visual System

The **Visual System** is a very experience-dependent hierarchical network, which therefore can undergo large reorganization or plastic processes [8]. Also, the extensive knowledge of its structure and its properties upholds the visual system as one of the finest models to study plasticity in the nervous system.

The eye can be divided into two segments: **anterior segment**, composed of the cornea, lens, iris and ciliary body and the **posterior segment**, made of the vitreous humour, retina and choroid [9] (Figure 1.1). The structures of the anterior segment play a role in the focus and transmission of the light onto the retina while components like the vitreous and the choroid humor are essential for pressure maintenance, physiological balance and ocular nourishment of the tissues [10].

Vision is a perceptual phenomenon that starts in the retinal neural networks, at the back of the eye [11]. Retina is a light-sensitive layered structure that receives information with different types of routing in central and peripheral vision. The central visual field information is relatively more processed by ventral visual pathways whereas the peripheral processing is mostly mapped by the dorsal pathways [12, 13]. This means that there is a clear distinction within the brain and the loss of central and periphery vision will lead to different patterns of damage and effects [14].

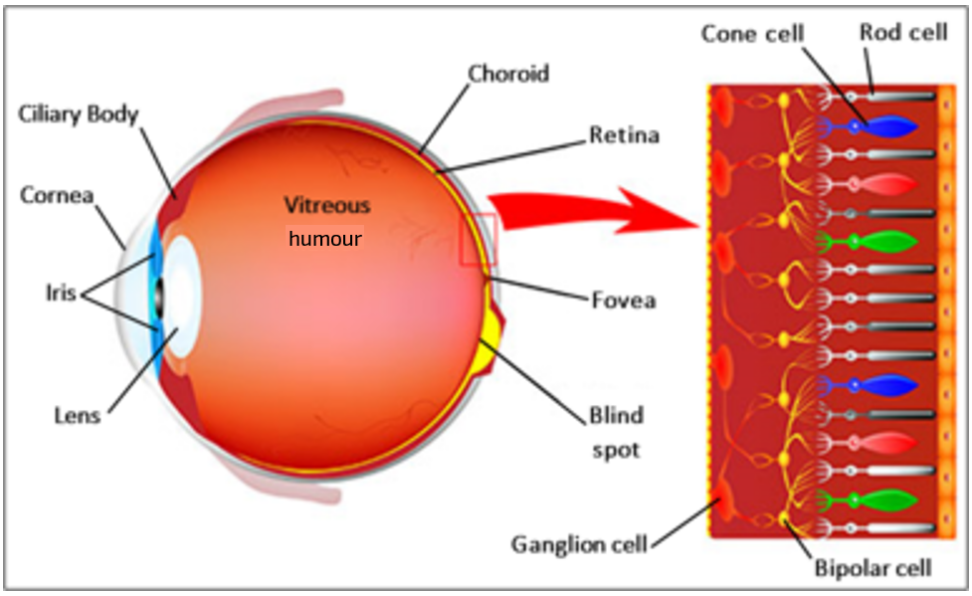

Figure 1.1: Representation scheme of the eye structure (left) and cellular organization of the retina (right), adapted from [15].

The sensory retina contains multiple layers of neuronal tissue that are connected through specialized synapses [9, 11] (Figure 1.1). The outer layer is light-sensitive and consists of photoreceptor cells, being composed of rods and cones [11]. Rods are responsible for the low-light vision and are the most abundant cells in the retina. Cones, on the other hand, provide colour vision and high spatial acuity [10].

Essentially, when light hits the retina, photransduction occurs and the photoreceptors signals are sent to bipolar cells, with lateral modulation by horizontal cells (also called retinal interneurons) which, thereon, send information, with lateral modulation from amacrine cells, to retinal ganglion cells (RGCs), the output neurons of the eye. RCGs fire action potentials which propagate throughout optic nerves until they reach the posterior part of the brain [11], the visual cortex in the occipital lobe. The visual cortex has three early visual areas: V1, V2 and V3, being V1 the visual area that first receives main sensory input from the optic nerve from the retina [16].

The full visual trajectory starting at the eye and ending in the occipital pole is represented in Figure 1.2.

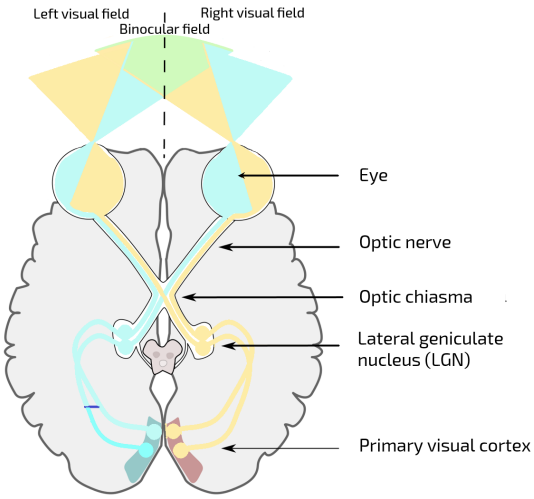

Figure 1.2: Retinocortical Pathway, adapted from [17].

1.3 Neuronal visual plasticity

In fact, even though early developmental plasticity is a widely accepted phenomenon, the concept of adult plasticity still sparks controversy due to the disparity in experimental observations [18].

Contradictory results can be found in animal studies following retinal lesions since the early days. In the 90s, Kaas et al. (1990), Chino et al. (1992) and Darian-Smith (1995) found that the primary visual cortex (V1) is capable of reorganization after parafoveal retinal lesions in adult mammals, cats and monkeys [19, 20, 21]. In 2008, Keck et al. also reported functional reorganization in the visual cortex of adult mouse based on the discovery that the Lesion Projection Zone (LPZ), a region that becomes unresponsive after retinal regions lesions, recovered its visual responsiveness within weeks to months [22]. In addition, and more recently, Botelho et al. (2014) also found significant topographic reorganization of V1 in adult monkeys, both inside and outside the cortical LPZ, occurring immediately after the retinal lesion [23]. However, Murakami et al. (1997) found no evidence of topographic reorganization of the LPZ in V1 in adult monkeys after monocular retinal lesions, using electrophysiological recordings [24]. The same conclusion can be found in Smirnakis et al. (2005) where they reported no indication of long-term cortical reorganization in adult monkeys using fMRI, since there was no significant change in

the signal across the V1 LPZ border, which was also confirmed with electrophysiological recordings [25].

Baseler and colleagues (2002) were the first to found evidence for V1 reorganization in adult humans due to abnormal retinal input. In their study with rod achromacy patients, a rare congenital form of colour deficiency that leads to cone malfunction affecting central vision, they reported that in patients the receptive fields of perifoveolar neurons surrounding LPZ have shifted towards the areas of V1 which were deprived of signals from the fovea [26].

Most studies have focused on diseases affecting the central vision, especially Macular Degeneration (MD). Therefore, the most contrasting results in the literature are reported in this disease. The following studies reported the absence of reorganization processes in primary visual cortex (V1): Sunness et al. (2004) described the case of an MD patient with a central scotoma affecting the inferior retina who had a loss of BOLD activity in the corresponding part of the visual cortex (V1 LPZ) while keeping the cortical activity corresponding to the superior retina [27]; Masuda et al. (2008) discovered that in patients with juvenile MD a stimulus-related task can activate V1 LPZ but this activation is absent while seeing the stimulus passively [28]. Moreover, in a study of Baseler et al. (2011) comparing MD patients (juvenile and age-related forms) with real retinal lesions and healthy controls with simulated retinal lesions there was no evidence of large-scale remapping in adults with MD, since the signals from a specific region from the LPZ in patients did not differ from signals in the control group [29].

The controversy associated with these results is related with the evidence of many other studies that found indications of plasticity in several neuro-ophtalmological disorders. Baker et al. studies, for example, demonstrated large-scale reorganization in individuals with MD. Accordingly, peripheral visual stimuli strongly activates foveal cortex in MD patients, but not in controls, and this reorganization is dependent on the complete loss of foveal function [30, 31]. Moreover, Dilks et al (2014) demonstrated that large-scale reorganization of visual processing is dependent on complete bilateral absence of input from fovea [32]. In addition, Schumacher et al. (2008) claimed that in MD there is extensive cortical V1 reorganization in response to a behavioural adaptation. When stimulating the

preferred retinal location (PRL), i.e. the functional peripheral region of the visual field used by patients to fixate instead of the lesioned fovea, the area representing central vision became more activated than when stimulating a peripheral non-PRL and also when comparing to peripheral stimulation in controls [33]. Also, Liu T. et al. (2010) reported similar results and associate the reorganization potential to age-onset and feedback signals that are related with attention [34]. However, even within the articles that suggest plasticity events there are also some inconsistencies. In Dilks et al. (2009) study they found that the reorganization existent in MD patients is not limited to the PRL since both PRL and not-PRL produce equal responses at V1 LPZ at the same eccentricity [35]. This finding goes against Schumacher et al. (2008) and Liu T. et al. (2010). Therefore, it is unclear if the reorganization in MD is driven by passive or use-dependent mechanisms, or even if plasticity events does occur in MD patients.

Reorganization phenomena in patients with Glaucoma, a disease that causes a loss of retinal ganglion cells (RGC) leading to the formation of scotomas (visual field areas unresponsive to visual stimulation) within the visual field of the affected eye, has also been evaluated and it is controversial. An fMRI study of Borges et al. (2015) showed reduced BOLD activation in the V1/V2 LPZ in the glaucomatous eye corresponding to the loss of visual function, suggesting that there is no V1/V2 plasticity in Glaucoma patients [36]. However, more recently, Zhou et al. (2017) study suggests that there is functional remapping in the visual cortex of patients with Glaucoma, since the areas of the parafovea activated were proven to be enlarged in patients and the cortical magnification factor was also higher in patients at small eccentricities. This could be associated to a remodeling process that exists as a response of the reduced peripheral visual fields [37].

It was not until 2010 that a study with Retinitis Pigmentosa (RP), a disease that affects the photoreceptors leading to the loss of peripheral vision, was made. Masuda et el. (2010), studied patients with Retinitis Pigmentosa and reported no V1 reorganization, since BOLD responses in foveal LPZ in the anterior calcarine in V1 only occur in the presence of a task-related stimulus and not when passively observing the same stimuli. Thus, the responses on the V1 LPZ of RP patients are task-related and not a result of reorganization due to the disease [38]. On the opposite, a new study with RP by Ferreira et al. (2017)

using functional magnetic imaging (fMRI) indicates a systematic visual field remapping in the primary visual cortex of RP patients that depends on the magnitude of the visual loss. They found an eccentricity shift of central retinal inputs to more peripheral locations in V1, whose pattern is consistent with shifting or expanding neuronal receptive fields into cortical regions with lower retinal input [1]. These differences may also depend on whether analyses focus in regions within or neighboring the LPZ. Indeed, Ferreira et al. (2019) have also recently identified an attentional effect including the LPZ irrespective of the remapping described above [39].

Most of the studies until now have focused on disease models of impaired central vision. For that reason, there is a lack of information in terms of cortical visual plasticity for diseases that affect peripheral vision.

Understanding the phenomenon of plasticity and/or reorganization can open doors to the development of treatments and rehabilitation procedures for neuro-ophtalmological and other cerebral diseases and also aid in evaluating materials and surgical techniques for eye interventions like refractive or cataract surgery [40]. Naturally, to be able to manipulate a certain neuronal pathway or even specific synapses known to be recruited after a particular event that produces negative effects on the brain would be of utmost importance in therapeutic and clinical interventions, improving the patient's quality of life [41].

1.4 A disease model of peripheral Visual Field degeneration: Retinitis Pigmentosa

Retinitis Pigmentosa (RP) is a rare inherited retinopathy affecting the photoreceptors' layer in the retina. It predominantly affects the rod photoreceptor cells but its atrophy gradually extends to the degeneration of cones [9, 42].

RP leads to the formation of severe visual lesion areas which causes partial to full blindness (scotomas, *localized areas of a severe visual defect*), especially in the periphery of the visual field (Figure 1.3) [1]. Even though the loss of visual field is typically peripheral, with the progression of the disease the central vision may also become compromised.

Other symptoms include loss of night vision. [9, 42].

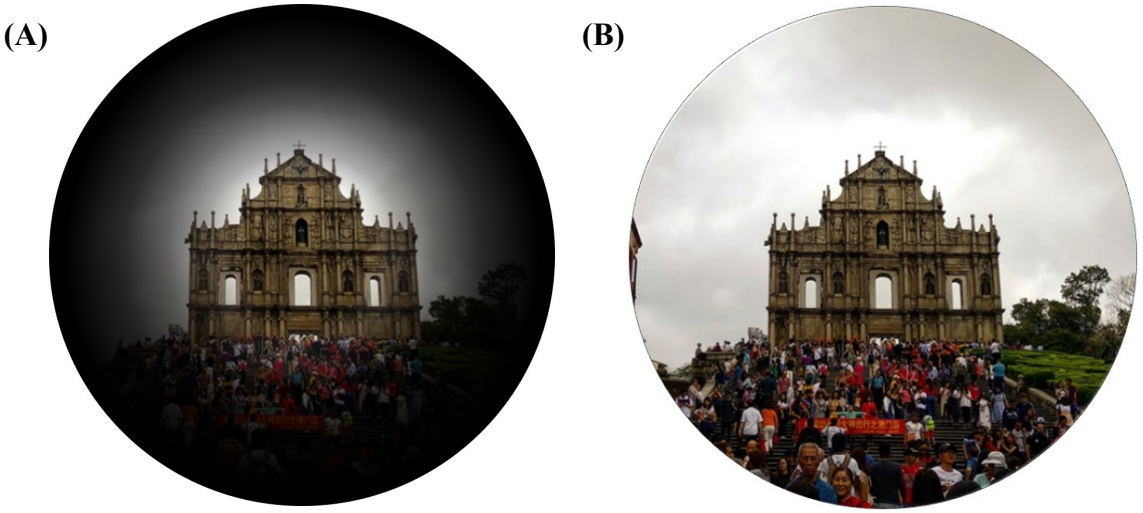

Figure 1.3: Simulation of the visual field perception of a person with RP (A) and a person with normal vision (B).

RP can be associated with other syndromes, such as Usher syndrome (syndromic RP), most commonly characterized by congenital hearing loss, or Bardet-Biedl syndrome [9, 42].

RP is a highly heterogeneous disease. Systemic RP is known to have mutations in 50 different genes while syndromic RP is associated with 12 gene mutations for Usher syndrome and 17 cause Bardet-Biedl syndrome [43]. The worldwide prevalence of this disease, syndromic and systemic, is of 1:3000 to 1:7000 people [42].

Currently, no cure for RP has been found, since there is still a lack of information about the mechanisms underlying photoreceptors' death [9].

Furthermore, the onset for RP can start early in childhood or later in adulthood, although symptoms typically manifest in adolescence [44]. Therefore, this makes RP a good model to study adult visual plasticity [40] and, thus, it is the disease model assessed in this work.

1.5 Retinotopy and Population Receptive Fields

Functional magnetic resonance imaging or functional MRI (fMRI) measures brain activity by detecting changes in the differential distribution of the blood flow to tissues with increased neural activity, which demand higher concentrations of oxygen. The information is based on the blood oxygenation level-dependent (BOLD) signal, that relies on the microvascular magnetic resonance signal on T2- and T2*- weighted images changes with the state of blood oxygenation: T2 measures the rate of loss of proton spin phase coherence, and T2* (local magnetic field homogeneity) is modulated by the presence or not of deoxyhemoglobin. The iron existent in hemoglobin is used as a magnetic susceptibility-induced T2*-shortening contrast agent, serving as a local indicator of functional activation [45]. Since oxyhemoglobin is diamagnetic it causes little to no distortion to the magnetic field but deoxyhemoglobin, on the other hand, is strongly paramagnetic and hence changes the local magnetic field. The microscopic field heterogeneities associated with deoxyhemoglobin lead to a destructive interference from the signal in a given voxel of brain tissue, which tends to shorten the T2* relaxation time. T2 and T2* region relaxation times of brain increase as the fraction of deoxyhemoglobin decreases [46]. In sum, when there is an increase of the flow of oxygenated blood resulting from enhanced neural activity, T2* becomes longer and the MRI signal intensity increases relative to the baseline [45].

Functional Magnetic Resonance Imaging allows the study of the brain activity *in vivo* and, as a result, can be used to indirectly investigate and understand visual plasticity phenomena [40].

Retinotopy is basically defined by the retinal topography in the visual cortex of the orderly representations of the visual field [47, 48]. Retinotopy or Phase-Encoded (or Travelling Wave) Retinotopic Mapping is a standard method to create travelling waves of cortical activation in order to distinguish retinotopic polar angle and eccentricity maps within each hemisphere, while using phase-encoded visual stimuli [49]. The polar angle allows the definition of the boundaries of the visual areas and the eccentricity the definition of the distance to the centre of the gaze.

In sum, it allows the localization of functional imaging data that clearly correlates with

the architecture of the visual system in each individual [50]. Hence, it is a powerful tool to investigate the differences of retinotopic properties of visual areas between healthy and unhealthy subjects [50].

In order to better study the properties of visual field maps an optimized technique named Population Receptive Fields (pRFs) was recently developed [51]. A population receptive field is the portion of visual field which upon a stimulus causes a response [52], changing its properties (size and location). The pRF technique allows the modeling of RF properties and the fitting of these models to the functional Magnetic Resonance Imaging time series [51].

It uses a model-driven approach to estimate the parameters that best explain the fMRI responses elicited by the stimuli in different visual locations at each voxel. This approach allows, for example, a more precise tracing of visual field maps using polar angle or eccentricity maps or even bars in different orientations [51] (Figure 1.4).

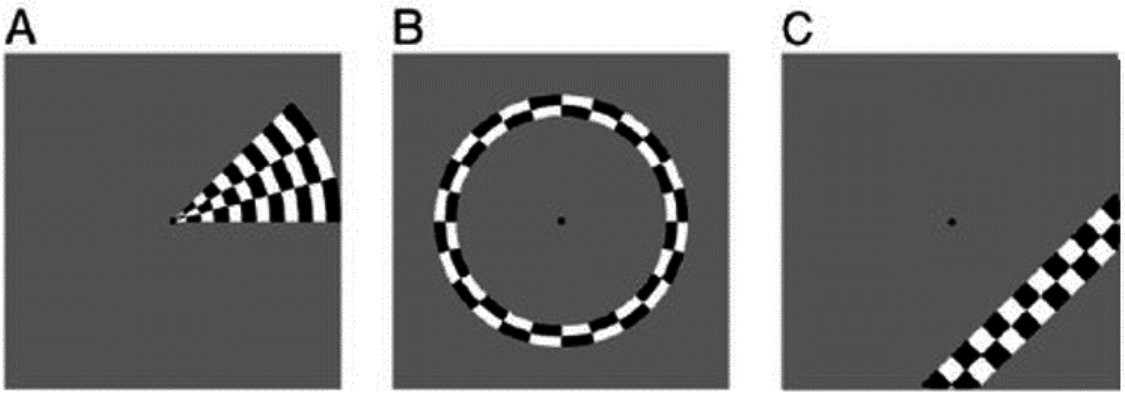

Figure 1.4: Different types of stimuli: moving (A) wedge, (B) ring and (C) bar, adapted from [53].

The most common method for the fitting applies a Gaussian model with three free parameters: the position of the population receptive field, given by x and y, and its size (i.e. standard deviation, σ), and is given by Equation 1.1 [54]:

$$g(x,y) = e^{-\frac{(x-x_0)^2+(y-y_0)^2}{2\sigma^2}} \tag{1.1}$$

These methods allow to study properties of populations of receptive fields of the visual

neurons, which may be markers of reorganization and, thus, can be used to study plasticity.

The purpose of this work was to determine whether neurosensory (visual) plasticity occurs in adult life of RP patients or if it is just an adaptive process. Therefore, a paradigm with scotomas' mapping in patients was used and tested with the pRF technique, while controls were stimulated with a regular stimulus and artificial scotomas to provide control of visual remapping.

2

Material and Methods

2.1 Participants

A total of 37 participants enrolled in this experiment belonging to three independent groups:

- **RP group:** This group was constituted by 12 individuals with Retinitis Pigmentosa (9 male, 3 female; mean age = 33.9 ±8.3 years; age range: $19 - 44$ years); 4 of this patients have Usher syndrome (USH, syndromic RP), characterized by a loss of hearing in addition to the vision loss;
- **Control group:** This group was constituted by 13 healthy controls (9 male, 4 female; mean age = 33.2 ±9.8 years; age range: $22 - 54$ years) who were stimulated with the *original* stimuli;
- **AS group:** This group was constituted by 12 healthy controls engaged in the Artificial Scotoma control experiment (9 male, 3 female; mean age = 34.0 ±6.7 years; age range: $24 - 44$ years). This group was submitted to stimulation by the *original* stimuli masked by the perimetric maps that corresponded to the visual field of a specific RP patient (details in the Section "2.3 Stimuli and Experimental Design").

The individual clinico-demographic and ophthalmological characterization of the participants are described in Table 2.1. For more details consult Appendix A.

Exclusion criteria included visual field diameter lower than 5 deg and/or visual acuity lower than 0.2 in both eyes, that would result in difficulty in fixation of the central cross during visual examinations and fMRI acquisitions.

Table 2.1: Clinico-demographic and ophthalmological characterization of the subjects cohort. Visual acuity was determined using a decimal chart. The extent of visual diameter was based on the static perimetry results by excluding absolute regions (black regions with sensitivity below 10dB).

* The selected eye was the dominant unless it had the lowest visual acuity.

ID	Group	Age (years)	Gender	Selected Eye*	Age of Onset (years)	Disease Duration (years)	Mean Visual Acuity (decimal)	Mean Visual Angle (diameter)
RP1	RP	19	M	L	7	12	0,6	13,75
RP2	RP	41	M	L	18	23	0,55	6,25
RP3	RP	35	M	L	6	29	0,7	10
RP4	RP	37	F	L	32	5	0,7	21,25
RP5	RP (USH)	34	F	R	14	20	0,65	9
RP6	RP	34	F	R	3	31	0,45	17,25
RP7	RP	23	M	R	16	7	0,58	8,25
RP8	RP	24	M	R	14	10	0,45	43
RP9	RP	31	M	L	2	29	0,6	47,25
RP10	RP (USH)	43	M	R	8	35	0,8	13,25
RP11	RP (USH)	42	M	R	14	28	0,6	8,25
RP12	RP (USH)	44	M	R	18	26	0,325	7,5
CNTR1	Control	22	M	L	-	-	1	48
CNTR2	Control	36	M	L	-	-	1	48
CNTR3	Control	41	M	L	-	-	1	48
CNTR4	Control	39	F	L	-	-	1	48
CNTR5	Control	30	F	R	-	-	0,83	60
CNTR6	Control	29	F	R	-	-	1,33	48
CNTR7	Control	24	M	R	-	-	1,33	48
CNTR8	Control	24	M	R	-	-	0,9	48
CNTR9	Control	33	M	L	-	-	0,8	48
CNTR10	Control	47	M	R	-	-	1,33	48
CNTR11	Control	26	M	R	-	-	1	48
CNTR12	Control	26	F	R	-	-	1	48
CNTR13	Control	54	M	R	-	-	1	60
AS1	Control Simulated	24	M	L	-	-	1	60
AS2	Control Simulated	39	M	L	-	-	0,9	48
AS3	Control Simulated	34	M	L	-	-	1	60
AS4	Control Simulated	39	F	L	-	-	1	60
AS5	Control Simulated	31	F	R	-	-	1	48
AS6	Control Simulated	34	F	R	-	-	1,3	48
AS7	Control Simulated	27	M	R	-	-	1,33	48
AS8	Control Simulated	25	M	R	-	-	0,9	60
AS9	Control Simulated	28	M	L	-	-	0,8	60
AS10	Control Simulated	44	M	R	-	-	1	48
AS11	Control Simulated	40	M	R	-	-	1	48
AS12	Control Simulated	43	M	R	-	-	1	60

Furthermore, static perimetry sensitivity maps were evaluated for all groups using a MonCv3 multifunction perimeter (Metrovision, France) with a standardized program. The individual perimetry maps of the RP patients are represented in Figure 2.1.

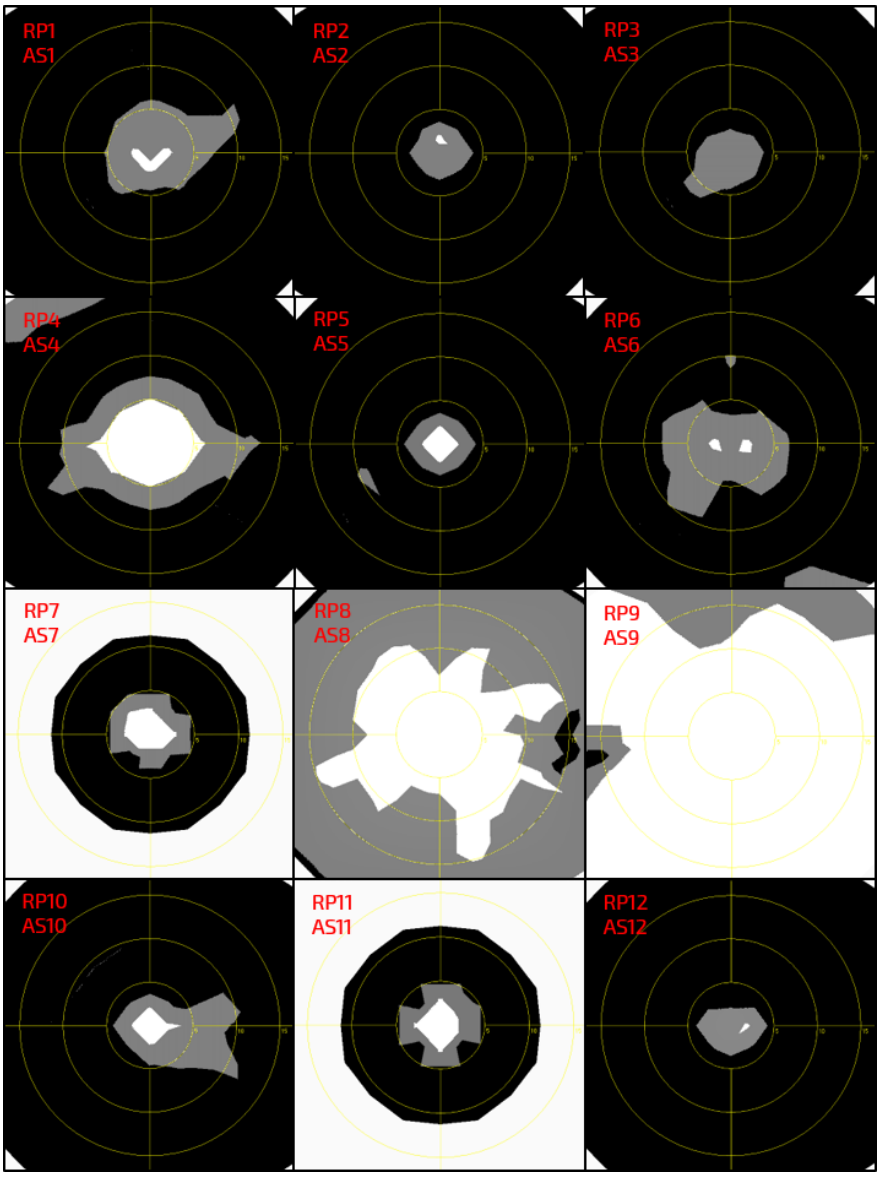

Figure 2.1: Individual static perimetry sensitivity maps of the Retinitis Pigmentosa (RP) patients (1-12). These static visual fields were used as masks for the participants of the artificial scotoma experiment.

All participants belonging to the control groups (Control and AS groups) were submitted to ophtalmological examinations that were performed by an experienced ophthalmologist to screen for eye disorders.

The recruitment of RP patients was performed in collaboration with the Ophthalmology

Unit at *Centro Hospitalar de Coimbra* (Portugal) whereas healthy controls were recruited from our volunteers database.

This experiment was approved by the Ethics Commission of Faculty of Medicine of University of Coimbra and followed the ethical standards of the Declaration of Helsinki.

2.2 Magnetic Resonance Imaging

Magnetic Resonance Imaging (MRI) data was acquired using a 3T scanner (Magneton TrioTim, Siemens AG, Erlangen, Germany) at the Portuguese Brain Imaging Network, with a 12-channel head coil. The protocol acquisition consisted on:

1. Two T1-weighted Magnetization-Prepared Rapid Acquisition with Gradient Echo sequences (MPRAGE): 176 slices with $1 \times 1 \times 1mm^3$ voxel size, Repetition Time (TR) 2.53 s, Echo Time (TE) 3.42 ms, Flip Angle (FA) 7 deg, Field Of View (FoV) $256 \times 256mm^2$;

2. Four functional acquisitions (two Polar Angle and two Eccentricity stimuli presented in alternated runs) using single-shot echo-planar imaging (EPI) acquired in the axial plane parallel to the Anterior Commissure (AC) - Posterior Commissure (PC) plane covering the occipital, temporal and frontal cortices, TR 2 s, TE 39 ms, interslice time (TI) 76 ms, FA 90 deg, FoV $256 \times 256mm^2$, 26 slices with $2 \times 2 \times 2mm^3$ voxel size and a 128×128 imaging matrix.

All anatomical images were assessed by a neuroradiologist in order to exclude clinical modifications.

2.3 Stimuli and Experimental Design

The visual stimuli was created using Matlab R2011b (The MathWorks, Inc., USA) and the Psychophysics Toolbox 3 extension (http://psychtoolbox.org/).

It was presented monocularly through MRI-compatible googles with refractive correction

(VisualSystem, NordicNeurolab, Norway) covering a maximum field-of-view of 23×30 degrees. The stimulated eye was the dominant eye, while the other eye was covered with a cotton patch. If the dominant eye had the least visual acuity, the other eye was chosen in order to avoid higher discomfort during the experiment. The dominant eye of each patient was determined using the Dolman hole-in-the-card test.

Stimuli were composed of a total of four runs, always starting and ending with a $12s$ baseline block consisting of a mid-grey background with a red fixation cross at the center of the screen. Each run had four 48s cycles containing either wedges or rings with a black and white checkerboard pattern flickering at a frequency of 8 Hz and with $\sim 100\%$ contrast (Figure 2.2).

Original stimuli consisting on a wedge rotating counter-clockwise (Figure 2.2 A) at a constant speed from the fixation cross mapped Polar Angle (PA) coordinates in the visual field. On the other hand, Eccentricity (ECC) was mapped by presenting rings slowly expanding from the fixation cross to the periphery (Figure 2.2 B). The order of the stimuli runs was PA-ECC-PA-ECC, which translates into an acquisition of two polar angle and two eccentricity runs of 216s.

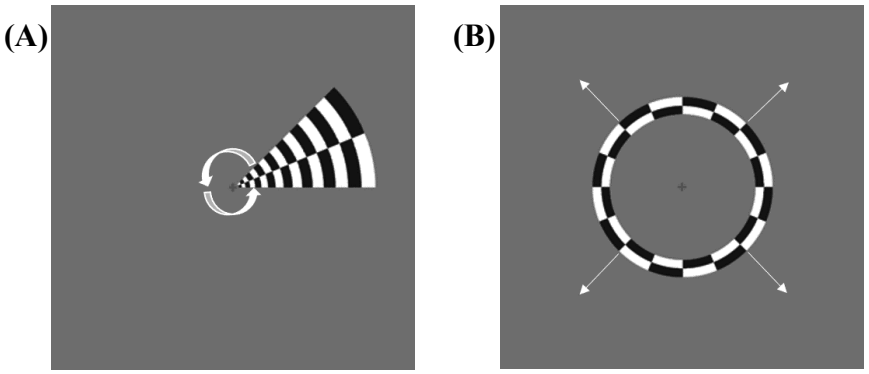

Figure 2.2: To study cortical visual maps, two retinotopic fMRI paradigms were used, comprising (A) a wedge rotating counter-clockwise and (B) an expanding ring stimuli, mapping polar angle positions and eccentricity positions regarding the center of the gaze, respectively.

A whole cycle of wedges (Polar Angle) and ring (Eccentricity) stimuli without intermediate fixation is depicted in Figure 2.3 and Figure 2.4, respectively.

On the other hand, control subjects participating in the artificial scotoma experiment ob-

served an adapted version of the *original* stimuli. Each control had his/her own polar angle and eccentricity stimuli overlaid by a mask corresponding to the defected visual field of the age- and gender-matched RP patient. The concept behind this masked stimulus was to try to mimic the visual field and perception of the RP patient when passively viewing the *original* stimuli artificially. An averaging smoothing filter was applied to the mask in order to create the soft blur seen in the images.

The frames (TR=2s) of a full cycle of polar angle and eccentricity stimuli without fixation images is represented in Figure 2.5 and Figure 2.6, respectively, for the AS group.

All the participants were instructed to fixate the central cross while passively viewing the stimuli.

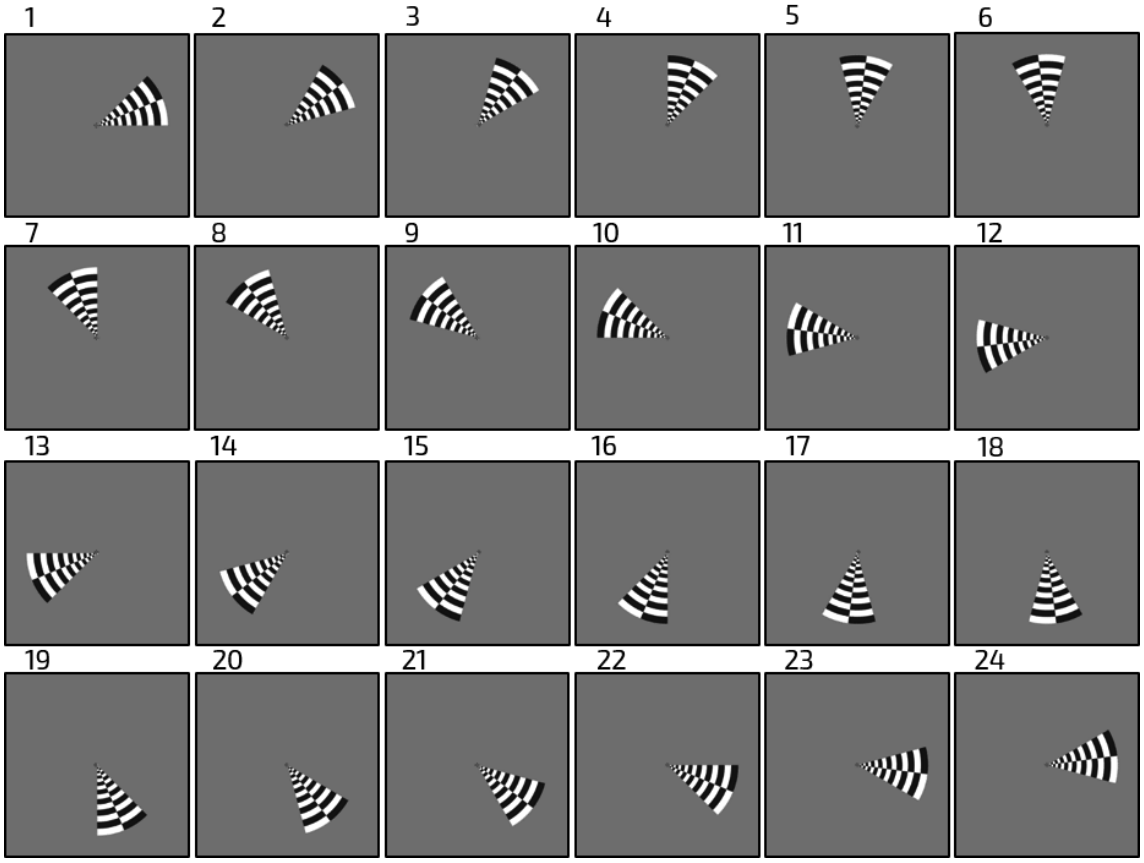

Figure 2.3: Illustration of a full cycle of wedge stimuli (*original* Polar Angle stimuli) for RP patients and controls.

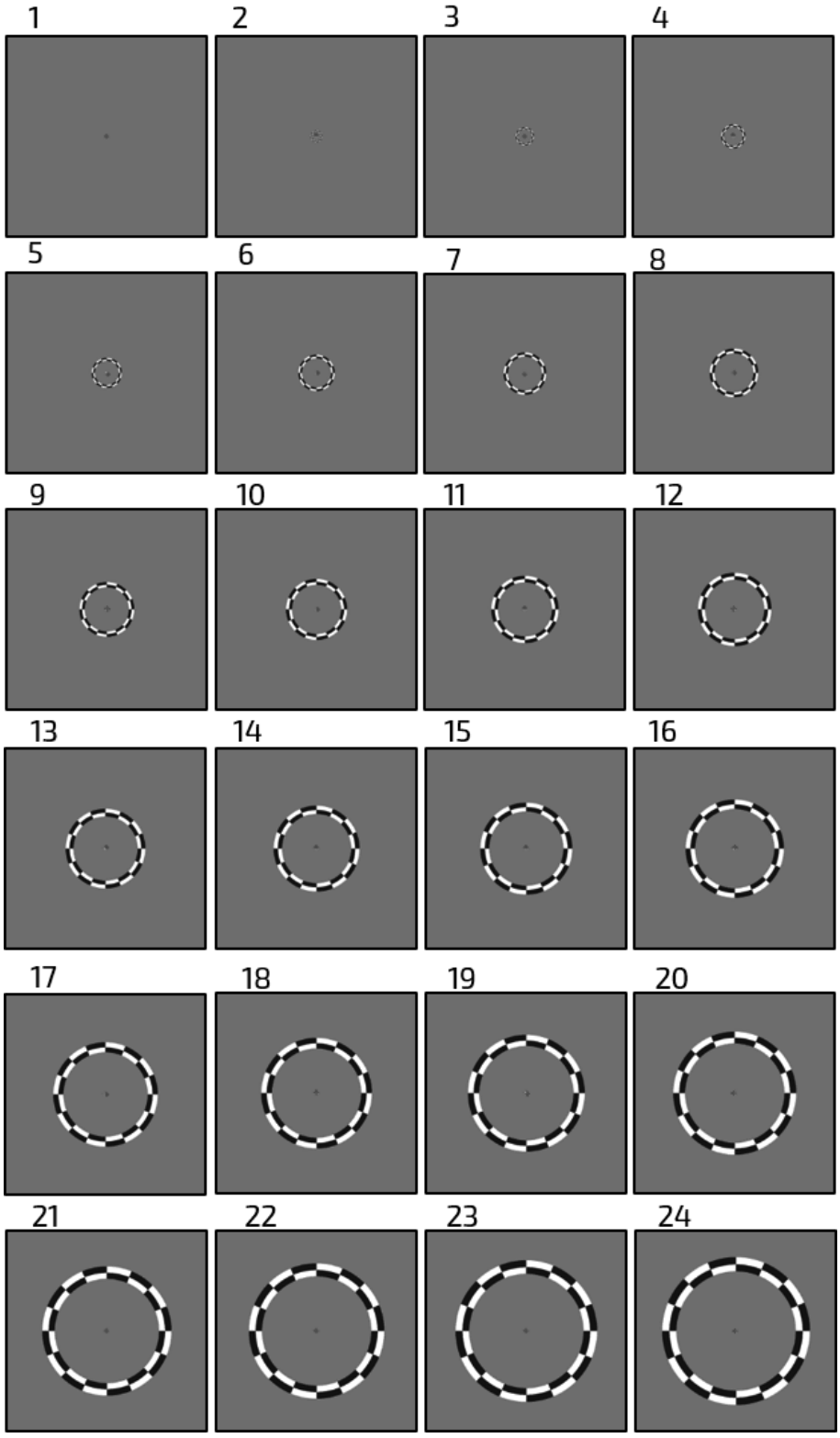

Figure 2.4: Illustration of a complete cycle of ring stimuli (*original* Eccentricity stimuli) for RP patients and controls.

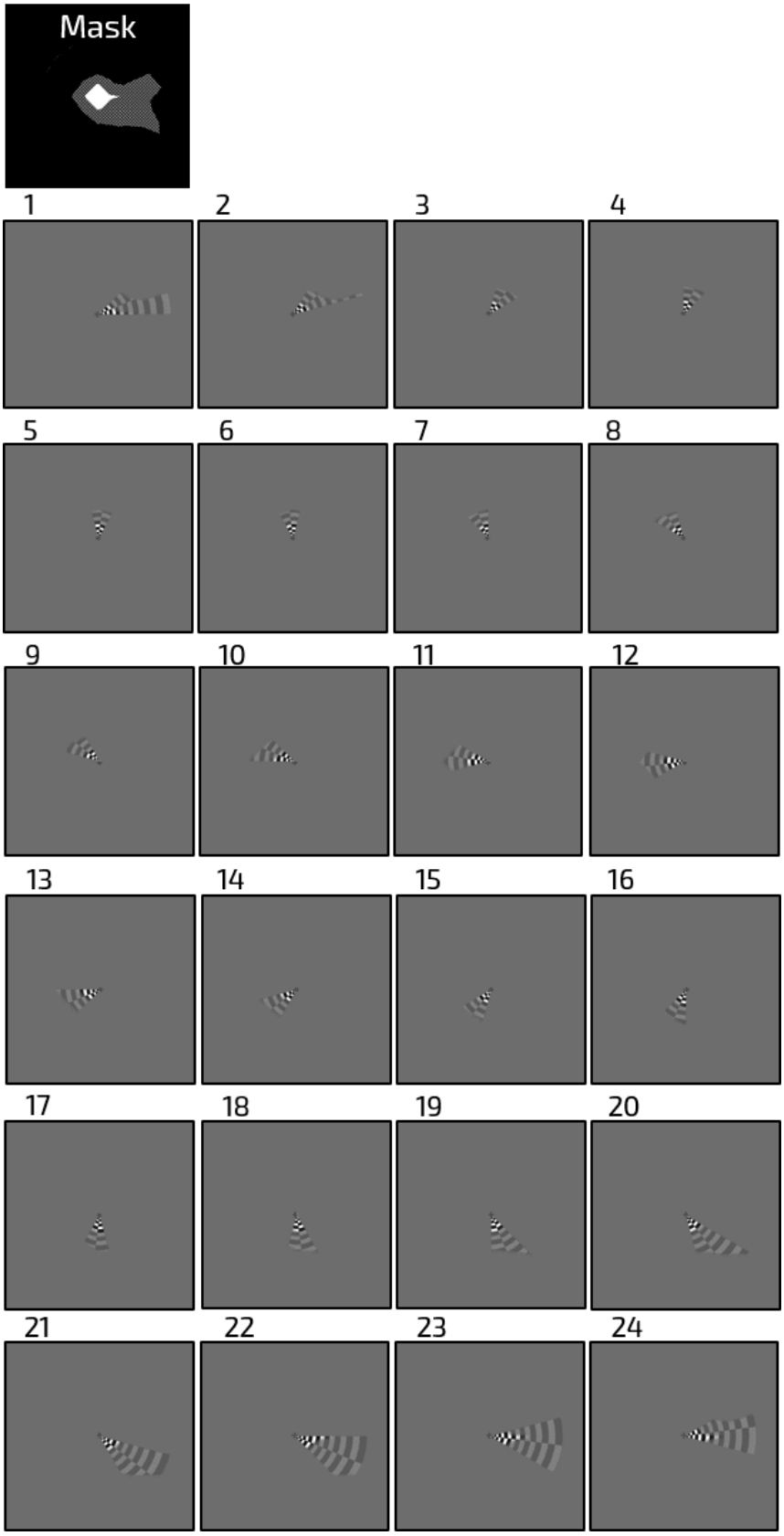

Figure 2.5: Illustration of a full cycle of wedge stimuli (Polar Angle) for an artificial scotoma participant (AS10).

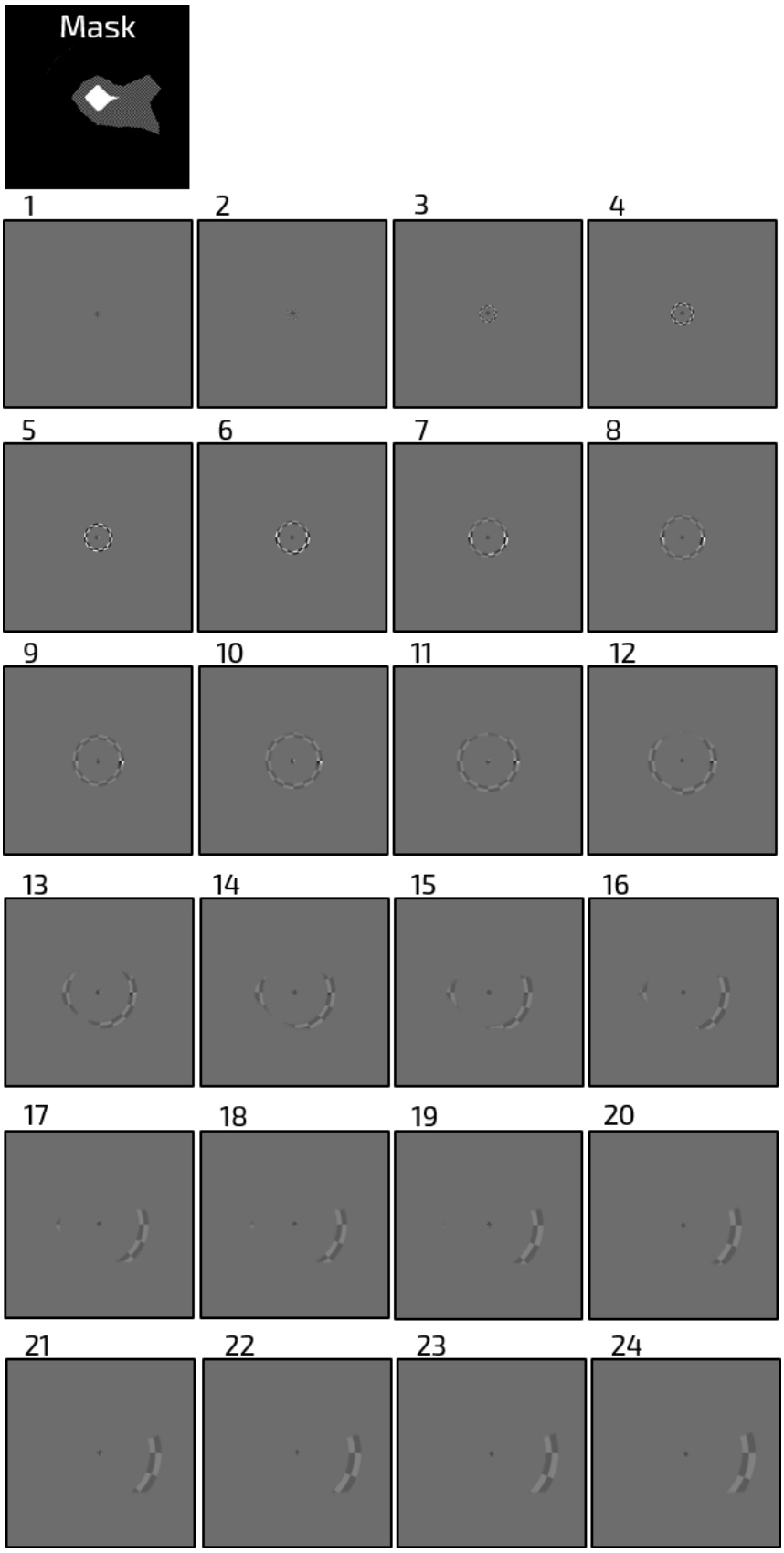

Figure 2.6: Illustration of a complete cycle of ring stimuli (Eccentricity) for an artificial scotoma participant (AS10).

2.4 Data Analysis

Image processing and analysis were executed with both Brain Voyager QX 2.6 and Brain Voyager 21.2 (Brain Innovation B.V., Maastricht, The Netherlands).

Matlab R2018a (The Mathworks, USA) and NeuroElf/BVQXTools Toolbox (http://www.neuroelf.net/) were used to estimate and evaluate the data from the retinotopic maps defined in BrainVoyager.

2.4.1 Anatomical Processing

For most cases, each subject had two anatomic MPRAGE acquisitions. In order to improve the signal-to-noise ratio (SNR), the anatomical images were averaged after performing the correction of the intensity inhomogeneities, through the estimation of bias fields and after the brain extraction.

Later, the volumes were aligned to the Anterior Commissure - Posterior Commissure (AC-PC) plane and transformed into Talairach coordinates. Thereon, the cerebral cortex was segmented into the cerebral fluid, white matter and grey matter using automatic segmentation tools in order to create the 3D inflated meshes of each hemisphere for better visualization of the functional data [18].

A summary of the main steps involved in the anatomical processing can be seen below in Figure 2.7.

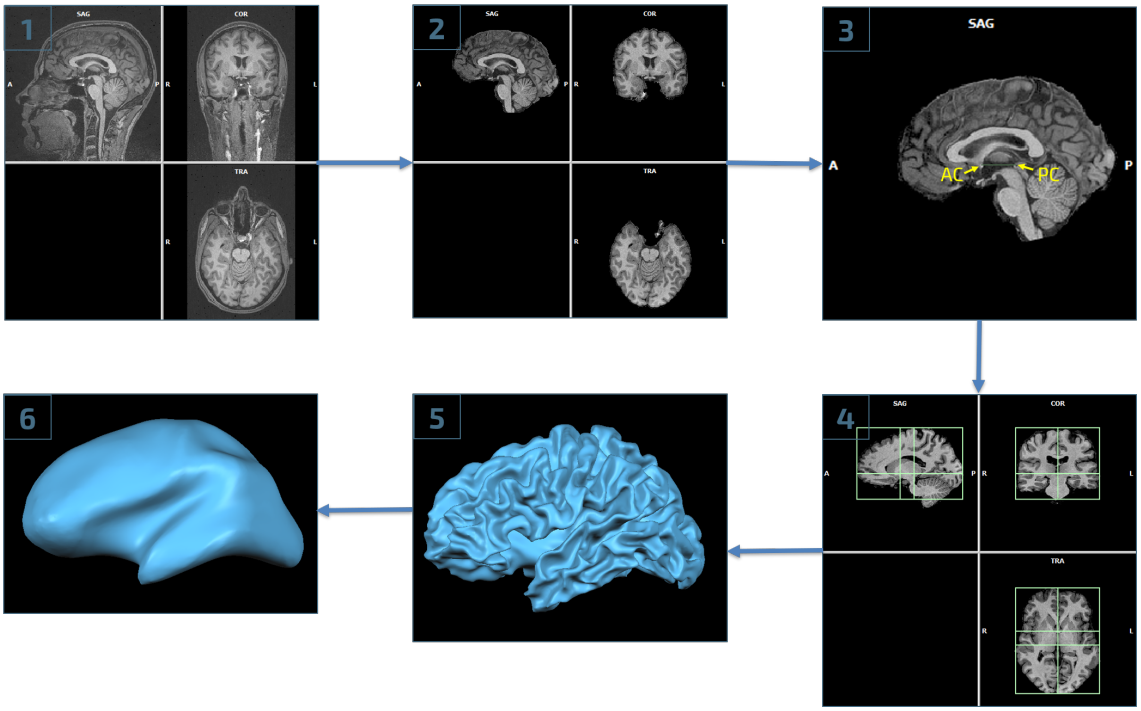

Figure 2.7: Illustration of the anatomical reconstruction steps. 1- Creation of the Volumetric Magnetic Resonance (VMR) dataset in the three anatomical planes; 2- Inhomogeneity correction of the VMR through the estimation of bias fields and brain extraction; 3- Anterior commissure - Posterior commissure (AC-PC) alignment; 4- Talairach (TAL) Registration; 5- Reconstruction of the surface mesh; 6- Inflation of the cortical mesh.

2.4.2 Functional Processing

The pre-processing of the fMRI datasets consisted on: Mean Intensity Correction, Slice Scan Time Correction, Motion Correction and Temporal Filtering (high pass, 2 cycles per run), with an intra-session alignment to the first volume of the first functional acquisition: the first Polar Angle. Since all the functional data were aligned to the first Polar Angle, the anatomical dataset was also co-registered to that same functional data (the first polar angle).

Moreover, and as a criterion, acquisitions whose subjects movement, whether from rotation or translation, had more than 3.0 degrees or 3.0 mm were removed in order to reduce noise. Consequently, the first eccentricity data from one subject of the RP group were eliminated from analysis.

Lastly, the data from two Polar Angle and two Eccentricity data runs were averaged to increase SNR.

2.4.3 Population Receptive Fields

Stimulus images had initially a resolution of 1366×768 pixels. They were cut into 300 $\times$ 300 pixels squared images in order to reduce computing time of the stimulus time courses file (STC), which comprise the information of both Polar Angle and Eccentricity stimuli.

Since the stimuli images to calculate pRFs had to be binary, for the AS group stimuli the gray part of the mask (Figure 2.1), corresponding to the area between preserved (higher) sensitivity areas (white) and non preserved lower sensitivity areas (black) was included in the AS experiment as an area of preserved sensitivity and, therefore, as white. The reason for the inclusion in the model is that these areas are still perceived by RP patients, just not completely. Hence, they can still hold important information.

Predicted Time courses (PTC) for the model were created using a grid of $30x$ and $30y$ positions extending from -11.5 to 11.5, creating a visual field of 23º $\times$ 23º. Moreover, we assumed that receptive fields sizes could range between 0.20 to 7 degrees, in 30 equal steps.

Since the region of interest is the occipital lobe, the analysis was limited to this region which, yet again, made the model estimation and fitting slightly faster.

In the pRF technique, the explained variance (R^2) was used as a quantitative measure of the goodness-of-fit of the model to the BOLD time series data. Therefore, and as a criterion, only voxels with $R^2 > 0.09$ ($R > 0.3$) were included in the analysis.

2.4.4 Statistical Analysis

Statistical analysis was performed using Matlab R2018a (The Mathworks, USA).

Normality assumption was tested using the Shapiro-Wilk test and parametric or equivalent non-parametric tests were applied accordingly.

For each analysis, the variables values of brain hemispheres were averaged in a region-of-interest (ROI) previously defined. No outlier removal criteria was considered for the analysis of both the mean values of the population receptive fields (pRFs) or the mean explained variance.

Repeated Measures ANOVA design requires normality and sphericity assumption, i.e., equal variances of the differences between all possible combinations of measurements [55]. Sphericity is tested using the Mauchly's test. In the cases where this supposition was not met, the epsilon ε value was calculated and the specific correction chosen as [18]:

- Huynh–Feldt, for $\varepsilon > 0.75$,
- Greenhouse–Geisser, for $\varepsilon < 0.75$.

A two-way repeated measures ANOVA was used to test the differences of 1) the slopes and 2) the intercepts (β_0) of the mean pRFs sizes along the 11 eccentricity bins between groups (RP and Control) and within visual areas V1, V2 and V3. Moreover, a repeated measures ANOVA design was performed independently in each visual area (V1, V2 and V3) to uncover the variation of the mean pRF sizes between groups (RP and Control) and within eccentricity zones (Central, Middle and Periphery).

A Mann-Whitney test was used to evaluate the differences of the median pRF size in the periphery of the primary visual area V1 between groups.

In a secondary analysis, we subdivided the RP group into two subgroups, regarding the maximum visual angle (va) perceived (RP, va $\leqslant 15$deg and RP, va > 15deg). A Kruskal-Wallis test was used to compare the mean pRF size in the periphery of V1 between the control group and RP subgroups.

Multiple comparison post-hoc tests with a Bonferroni correction were performed when necessary.

Inferential statistical analysis were performed with two-tailed hypothesis testing at a 5% significance level.

3

Results

3.1 Analysis of the participants sample

Firstly, we verified matching the frequencies of "*Gender*" and "*Chosen Eye*" (the selected eye used for monocular stimulation in MRI procedures) between groups of participants (RP, Control and AS). Two chi-squared tests were calculated: one for "*Group*" and "*Gender*" ($\chi^2(2) = 0.142$, $p = 0.931$) and another for "*Group*" and "*Chosen Eye*" ($\chi^2(2) = 0.036$, $p = 0.982$). Therefore, Gender (male/female) and the selected eye (right/left) were equally distributed in the three groups.

Afterwards, *age* and the mean *visual acuity* (VA) were compared between the three groups (RP, Control and AS). The ANOVA for age as the independent variable revealed no statistical differences between groups ($F(2{,}34) = 0.079$, $p = 0.924$). The Kruskal-Wallis test for visual acuity as the independent variable, however, showed, as expected, that there is a statistically difference of the median VA between, at least, two groups ($\chi^2(2) = 24.08$, $p = 4.102 \times 10^{-6}$). A *post-hoc* revealed that groups RP and Control (RP-Control, $p = 2.369 \times 10^{-5}$) and RP and Artificial scotoma (RP-Artificial Scotoma, $p = 8.887 \times 10^{-5}$) have statistically different medians, with RP group having lower visual acuity when compared to Control and the AS group, as expected.

3.2 Population Receptive Fields Analysis

The population receptive field (pRF) method returned six statistical maps related to the model fitting procedure: **R** (squared root of the explained variance), the **size** (standard deviation), the **x position**, the **y position**, the **eccentricity** and the **polar angle** for each selected hemisphere of a single participant.

An example of the obtained maps using the pRF technique is shown in Figure 3.1. It illustrates the maps of size, eccentricity and polar angle of the control CNTR4, the RP patient RP4 and AS participant AS4, for both left and right hemispheres. The mask of AS4 corresponds to the visual field of RP4 (Methods section, Figure 2.1).

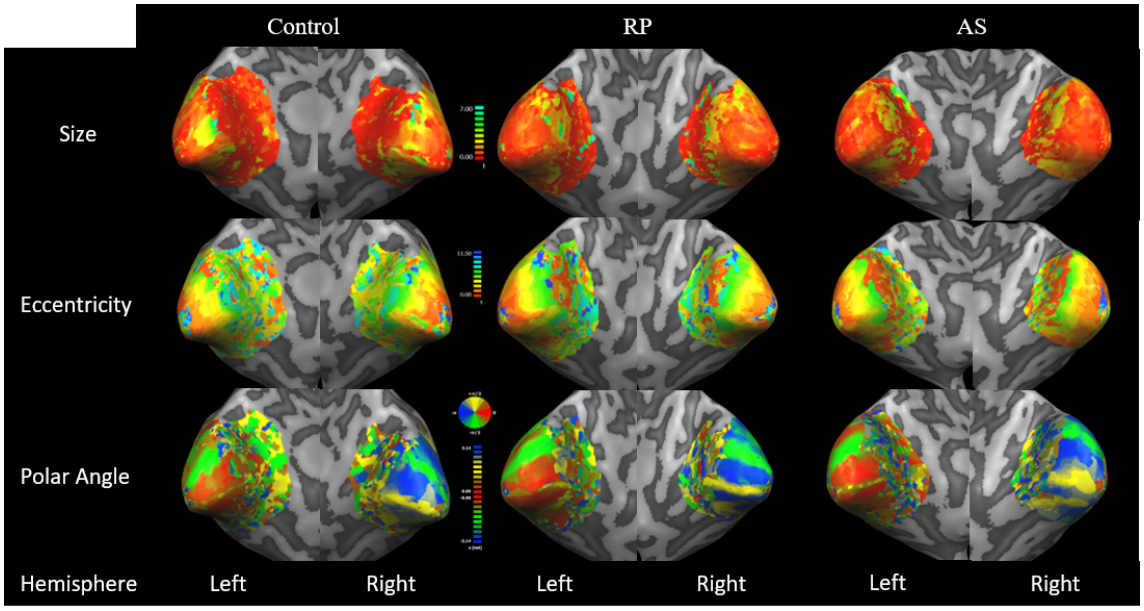

Figure 3.1: Illustration of the obtained maps that characterize the population receptive fields in terms of (upper row) **size**, (middle row) **eccentricity** and (bottom row) **polar angle** of a control (CNTR4), a patient with RP (RP4) and an artificial scotoma control (AS4). Maps are presented in a pseudo-colour code: **size** varies between 0 (red) and 7 (light blue) degrees of visual angle; **eccentricity** ranges from 0 (red) to 11.5 (dark blue) degrees of visual angle; **polar angle** alters from -3.14 (dark blue) to 3.14 (dark blue) radians. Both hemispheres are represented.

3.2.1 Difference in the patterns of pRF size along eccentricity and visual areas suggest loss of convergence in RP

There are two main ways to study plasticity using retinotopic maps, based on the approaches from animal studies: one is to study the change the receptive fields regarding its position (migration) or its size. Accordingly, we compared the sizes of the pRFs within visual areas V1, V2 and V3 between the control group and the RP group.

Firstly, we defined functionally retinotopic areas V1, V2 and V3 in each hemisphere of each participant of the control and the RP group. Using the coloured polar angle map obtained from the pRF modeling, the visual areas were manually defined over the inflated meshes, that resulted from the anatomical reconstruction, using BrainVoyager's drawing tools. These areas were considered regions of interest (ROIs) and used as masks for the analysis of the receptive field sizes later on. A representative example of the definition of the limits of the visual areas can be seen in Figure 3.2 below. Dorsal, V2d, V3d, and ventral, V2v, V3v sub-regions were merged into complete representations, V2 and V3, respectively.

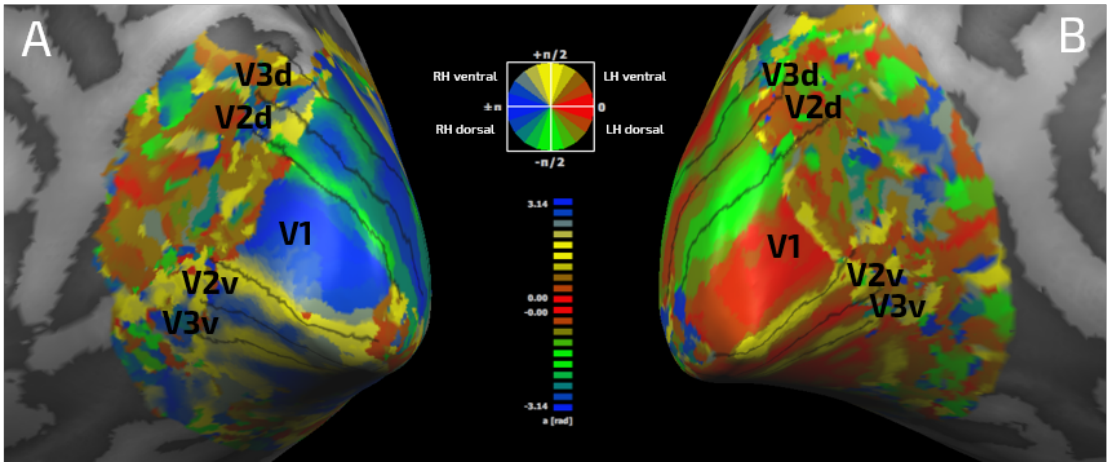

Figure 3.2: Representation of the definition of the borders between visual areas on the (A) right hemisphere and (B) the left hemisphere using Polar Angle maps.

In order to assess how the sizes evolve within each visual area, eccentricity was divided into eleven bins from 0.5° to 11.5° of visual angle, each spanning 1°. Thereafter, we calculated the mean pRF sizes in each bin and averaged the respective bins from each visual

area of each hemisphere for both the RP (Figure 3.3) and the Control (Figure 3.4).

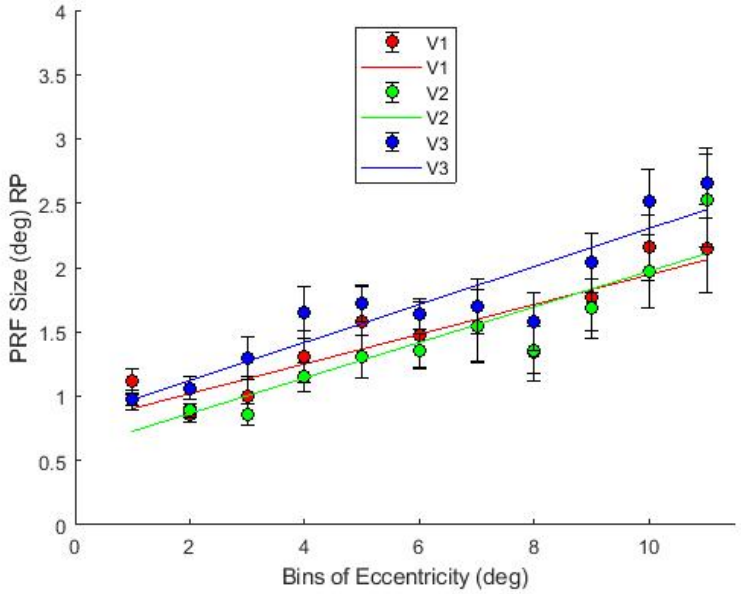

Figure 3.3: Representation of the mean pRF size (degrees) within each eccentricity degree (step: 1º) for each visual area (mean of both hemispheres), V1 (red), V2 (green), V3 (blue) for the RP group. For each visual area a linear fit procedure was performed. Error bars denote standard error of the mean (SEM).

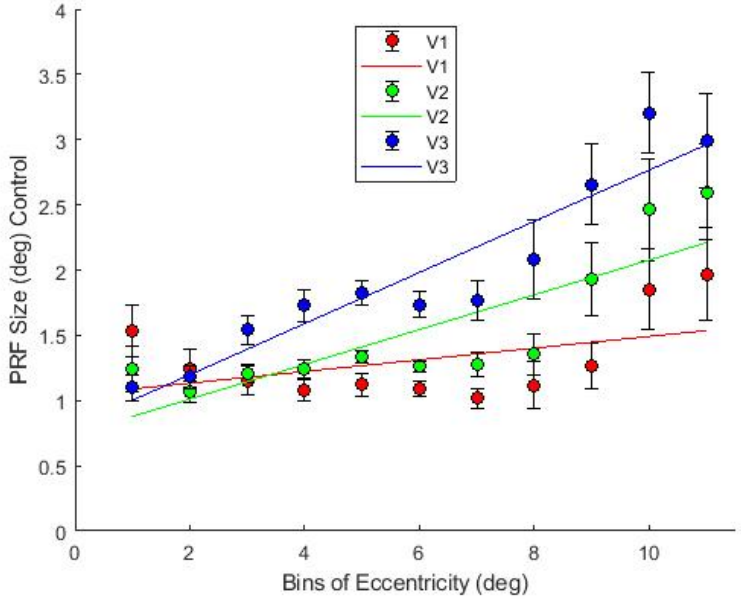

Figure 3.4: Representation of the mean pRF size (degrees) within each eccentricity degree (step: 1º) for each visual area (mean of both hemispheres), V1 (red), V2 (green), V3 (blue) for the Control group. For each visual area a linear fit procedure was performed. Error bars denote the SEM.

Subsequently, and due to the fact that we wanted to compare the within and between differences of pRF sizes of each visual area of each group, we decided to analyse the *slope* and *intercept* values (β_0) of the simple linear regression line fitted to the mean size values within each eccentricity bin. All the fitting lines are represented in Figure 3.3 and in Figure 3.4 for the RP and the control group, respectively.

After confirming the normality and the equality of the variances of the data, two repeated measures ANOVA were then performed.

The first consisted on the analysis of *slope* values of the fitting lines. Since we wanted to compare between groups (RP and control) and within visual areas (V1, V2 and V3), the repeated measures ANOVA was designed with *Group* as the between-subjects factor and *Visual Area* as the within-subjects factor. The resulting estimated marginal means of the slopes are depicted in Figure 3.5.

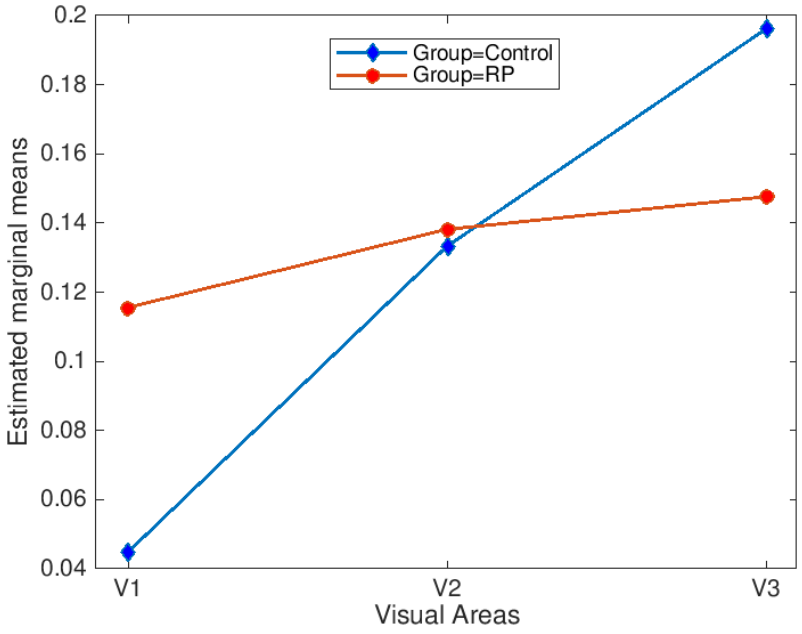

Figure 3.5: Plot of the estimated marginal means of the slope values of the regression lines of the visual areas V1, V2 and V3 (fitting of the mean pRF sizes along eccentricity bins) in the RP (red circles) and control (blue diamonds) groups.

There was a statistically significant interaction between Group and Visual Area ($F_{interaction}$ (2,46)$= 3.553$, $p = 0.037$) and a significant effect of Visual Area ($F_{visual\,area}(2,46) = 8.492$, $p = 7.262 \times 10^{-4}$). On the other hand, no effect between groups was found ($F_{group}(1,23) = 0.128$, $p = 0.724$). *Post-hoc* tests showed that the main effects found

between visual areas come from differences between V1 and V2 (V1-V2, $p = 0.036$) and V1 and V3 (V1-V3, $p = 0.006$).

A repeated measures ANOVA was applied on the values of β_0 of the fitting lines with the same between-subjects and within-subjects factors as previously. The estimated marginal means for the mean β_0 values for each visual area of each group are represented in Figure 3.6.

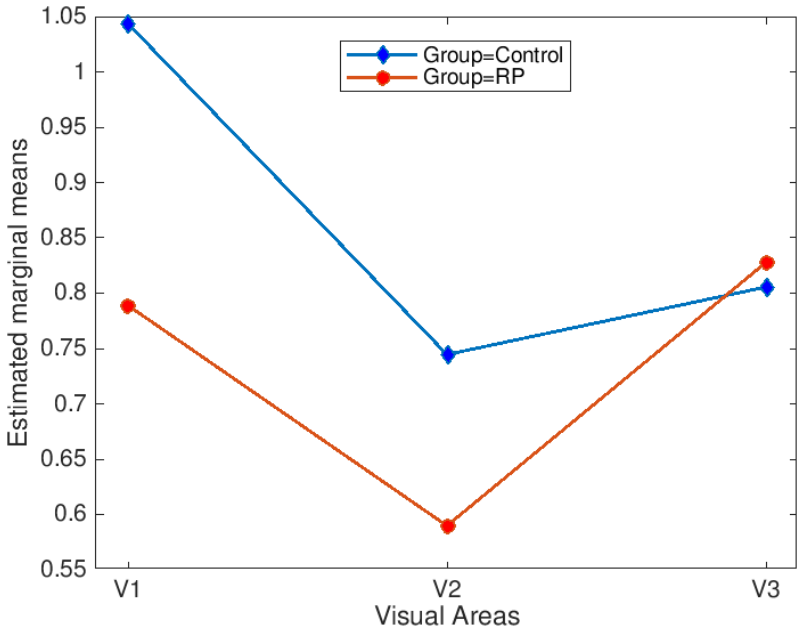

Figure 3.6: Plot of the estimated marginal means of the intercept values (β_0) of the regression lines of the visual areas V1, V2 and V3 V3 (fitting of the mean pRF sizes along eccentricity bins) in the RP (red circles) and control (blue diamonds) groups.

There was a significant main effect of Visual Area ($F_{visual\,area}(2,46) = 4.388, p = 0.018$). At the same time, no significant Group effect ($F_{group}(1,23) = 1.779$, $p = 0.195$) nor interaction effect was found ($F_{interaction}(2,46) = 1.372, p = 0.264$). *Post-hoc* tests with a Bonferroni correction showed that the main effect on visual areas were due to differences in the mean β_0 of V1 and V2 (V1-V2, $p = 0.012$).

These results, in particular the ones resulting from slope analysis, suggest a loss of convergence along visual areas and within the visual areas of the RP group.

We then hypothesized that the loss of convergence would be worse for the patients with smaller visual fields. Therefore, we divided the RP into two subgroups with a threshold of

visual angle of 15 degrees (*RP, va* $\leqslant 15$*deg* (n=8); *RP, va* > 15*deg* (n=4)) [1]. The results are indicative that the loss of convergence is clearer in patients with smaller visual angles, i.e., with the worst visual fields (Appendix B).

A repeated measures ANOVA between the subgroups of RP and within visual areas V1, V2 and V3 revealed, however, no statistically significant effects, probably due to our low statistical power.

3.2.2 pRF size is higher in peripheral representations of V1 in patients suggesting compensatory mechanisms

RP is a disease that causes blindness in the peripheral visual field. Accordingly, if reorganization really exists, we would expect to see bigger population receptive fields in the cortical regions mapping the peripheral areas of the visual field. The primary visual area V1 is the first cortical visual area to receive massive retinal sensory input. Therefore, we defined "*Periphery*" as the cortical zone mapping eccentricities from 7.5 to 11.5 deg [56] and calculated the mean pRF size of the peripheral representation in V1 for each group (Figure 3.7).

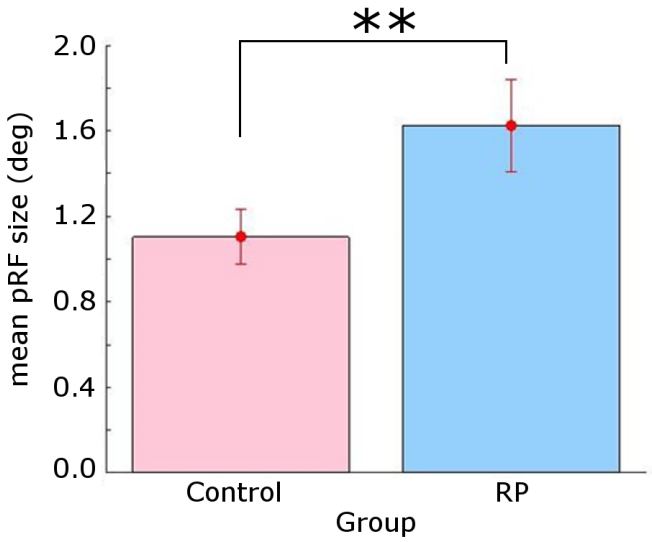

Figure 3.7: Representation of the mean pRF size (degrees) in the peripheral representation of V1 for both RP and control groups. The RP group had higher pRF sizes in the peripheral representations of V1 when compared to the Control group. Error bars denote the SEM. $^{**}p < 0.05$.

A Mann-Whitney U test was carried out to statistically evaluate whether the pRF size in the periphery of V1 was significantly different between the two groups (RP and Control). The medians between groups were statistically significant ($N = 25$, $U = 28$, $p = 0.007$), being higher in the RP group. This corroborates our hypothesis that the pRF sizes grow bigger in the periphery of V1 in order to compensate for the decrease in information load into V1, which leads us to believe that reorganization exists in patients with RP.

As before, if the reorganization occurred along to the disease progression, i.e. as the visual field gets gradually smaller, the pRF sizes would also progressively become larger in the periphery.

Once again, we studied the behaviour of the mean pRF size between the two RP subgroups (*RP, va* $\leqslant 15$*deg* ($n = 8$); *RP, va* > 15*deg* ($n = 4$)) and controls (Figure 3.8). As expected, the RP patients with a lower visual angle (inferior or equal to 15deg of diameter) have bigger population receptive field sizes in the peripheral representations on V1.

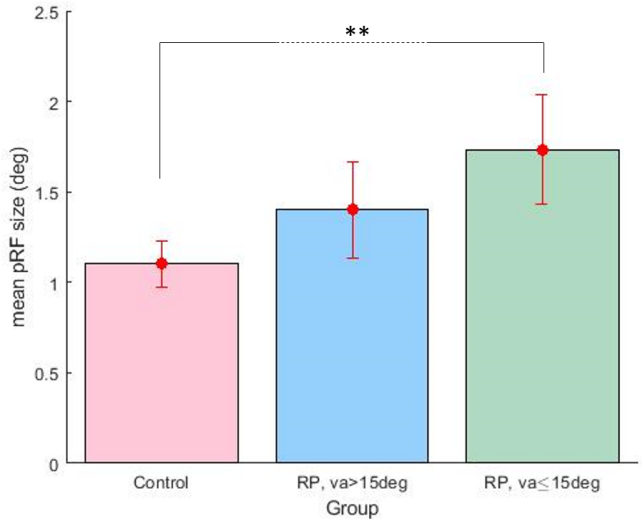

Figure 3.8: Mean pRF size (deg) in the peripheral representation on V1 for the Control group, the RP subgroup with a visual angle (va) greater than 15deg of diameter (RP, va>15deg) and the RP subgroup with va lower or equal to 15deg (RP, va $\leqslant$ 15deg). Error bars denote the SEM. **$p < 0.05$.

The Kruskal-Wallis test showed that the median of at least two groups are statistically different ($\chi^2(2) = 7.547$, $p = 0.023$). A *post-hoc* test revealed that the biggest significant difference was between the medians of the control group and RP subgroup with visual

angle inferior or equal to 15deg (Control-RP (va$\leqslant$ 15 deg), $p = 0.025$).

Our main hypothesis focused on the peripheral representations of the cortical V1, due to the fact that the periphery is the first and most affected region in RP and V1 is the first visual area to receive the bulk retinal input. Although we confirmed our main hypothesis, other alterations could have occurred in representations of other areas of the visual field (other eccentricities) and in other visual areas.

Accordingly, we first separated the eccentricity bins in three zones according to the distance to the centre: "*Central*" (0.5 to less than 2.5 deg), "*Middle*" (2.5 to less than 7.5 deg) and "*Periphery*" (7.5 to 11.5 deg) [56]. Then, we calculated the mean pRF sizes for each Visual Area along the different zones on each group. This data are plotted in Figure 3.9 and in Figure 3.10 for the RP and the Control group, respectively.

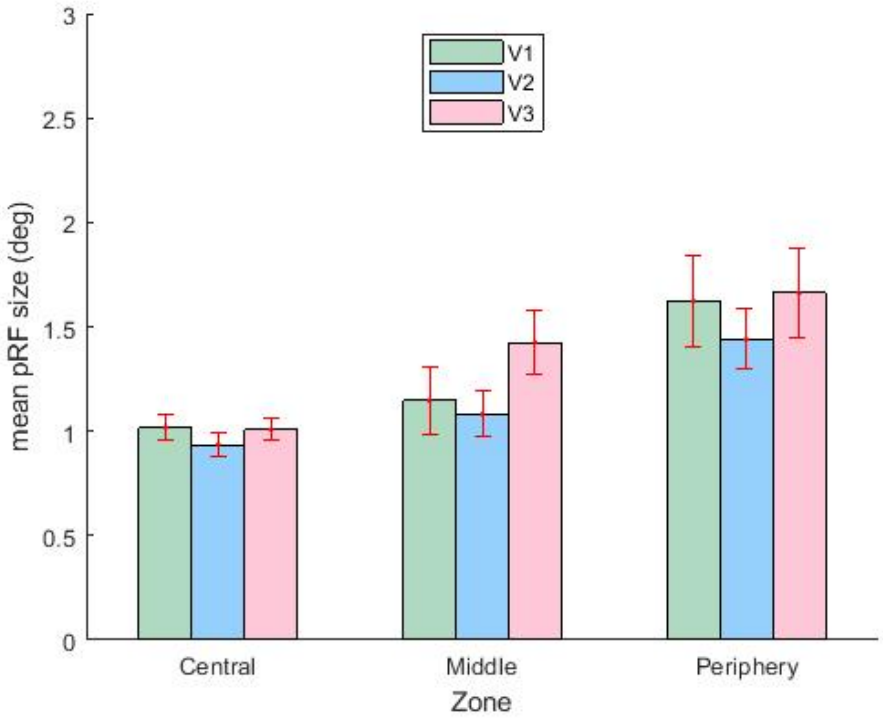

Figure 3.9: Mean pRF size in each eccentricity zone (central, Middle or Periphery) of the visual areas V1 (green), V2 (blue) and V3 (pink) of the RP Group. Error bars denote the SEM.

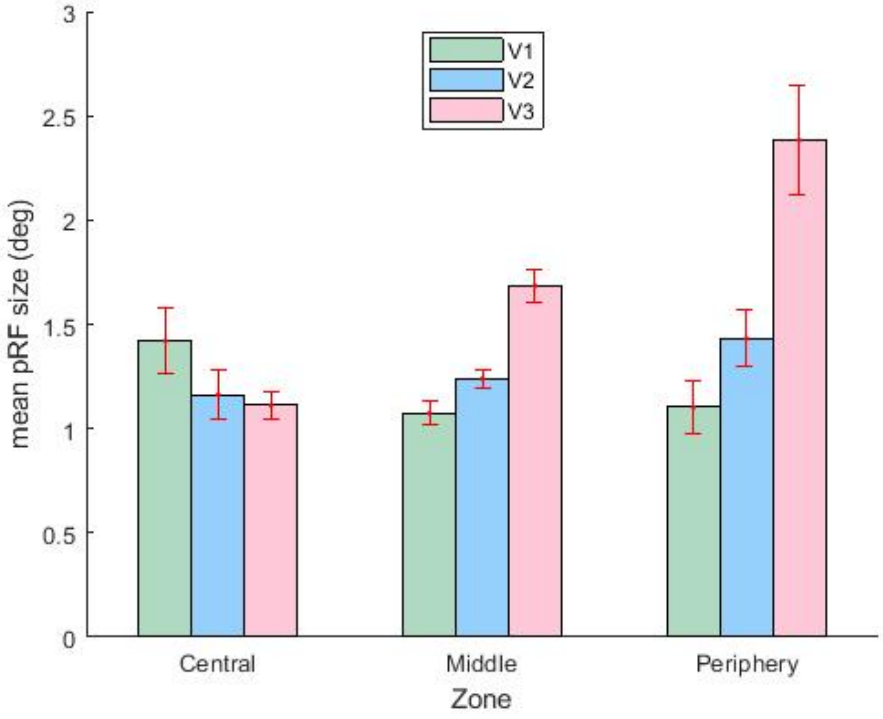

Figure 3.10: Mean pRF size in each eccentricity zone (central, Middle or Periphery) of the visual areas V1 (green), V2 (blue) and V3 (pink) of the Control Group. Error bars denote the SEM.

A repeated measures ANOVA was performed for each visual area independently, setting "*Group*" (RP and Control) as the between-subjects factor and "*Zone*" (Central, Middle and Periphery) as the within-subjects factor.

V1: The repeated measures ANOVA for V1 (Figure 3.11) revealed a significant interaction between Group and Zone ($F_{interaction}(2,46) = 5.892$, $p = 0.005$). However, no main effect of Zone ($F_{zone}(2,46) = 1.782$, $p = 0.180$) nor Group effect ($F_{group}(1,23) = 0.263$, $p = 0.613$) were detected.

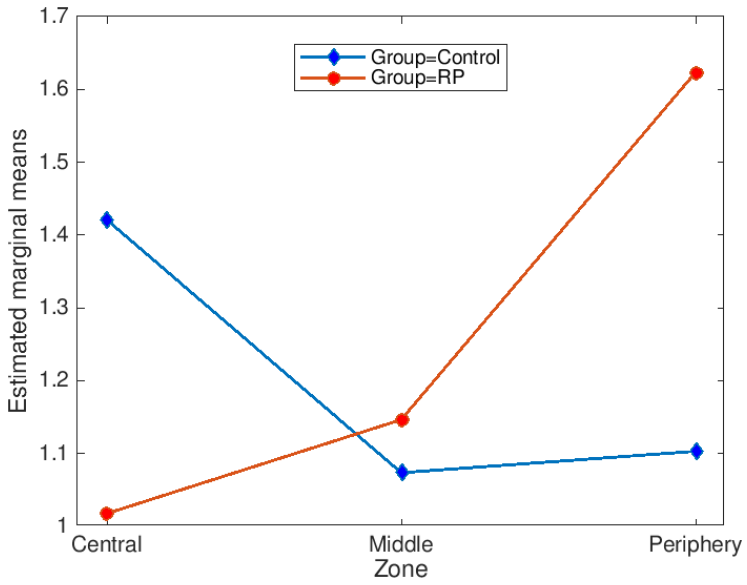

Figure 3.11: Estimated marginal means of pRF size in V1 between RP (red circles) and Control (blue diamonds) groups and within Central, Middle and Periphery zones.

V2: The repeated measures ANOVA of visual area V2 (Figure 3.12) shows that there is a significant Zone effect ($F_{zone}(2,46) = 9.761$, $p = 0.0003$) but no Group effect $F_{group}(1,23) = 1.275$, $p = 0.275$) nor interaction between factors ($F_{interaction}(2,46) = 0.896$, $p = 0.415$). Multiple comparisons testing between Zones in V2 revealed that the mean pRF sizes were significantly higher in the Periphery compared to both the Central zone (Central-Periphery, $p = 0.004$) and the Middle zone (Middle-Periphery, $p = 0.003$).

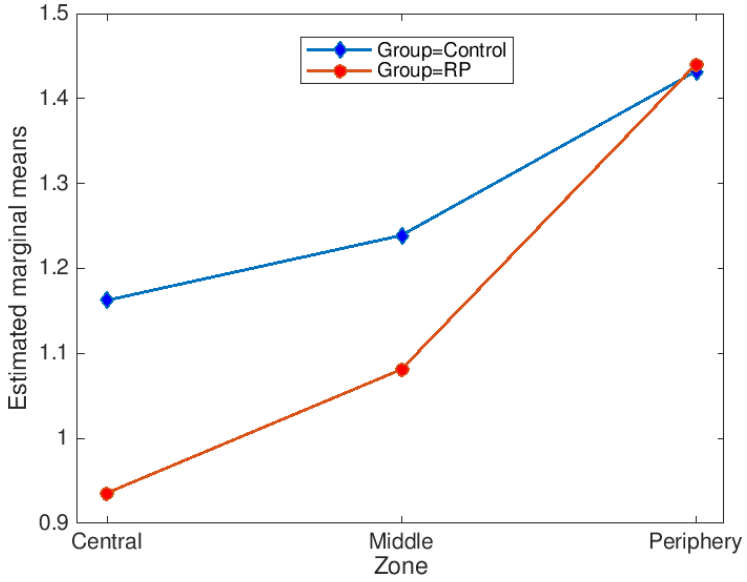

Figure 3.12: Estimated marginal means of pRF size in V2 between RP (red circles) and Control (blue diamonds) groups and within Central, Middle and Periphery zones.

V3: Lastly, we analysed the mean pRF size values in V3. The repeated measures ANOVA for V3 (Figure 3.13), with the same factors as the last two, showed a significant Group ($F_{group}(1,23) = 4.889, p = 0.037$) and Zone ($F_{zone}(2,46) = 25.50, p = 2.412 \times 10^{-6}$) effect. However, no interaction ($F_{interaction}(2,46) = 2.827, p = 0.090$) was found. Multiple comparisons testing was performed to understand the direction of the differences between the zones. All zones had statistically different mean pRF sizes, i.e., Central and Middle zones (Central-Middle, p=2.315×10^{-5}), Central and Periphery zones (Central-Periphery, p=2.124×10^{-5}) as well as Middle and Periphery zones (Middle-Periphery, $p = 0.008$). Mean pRF sizes were higher in Periphery and lower in Central representations. Overall, Control group exhibited higher pRF sizes across eccentricity zones.

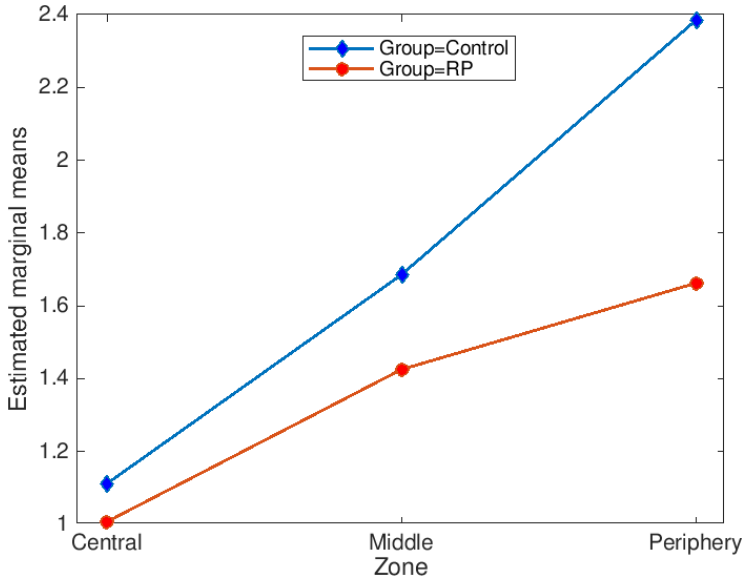

Figure 3.13: Estimated marginal means of pRF size in V3 between RP (red circles) and Control (blue diamonds) groups and within Central, Middle and Periphery zones.

3.3 Artificial Scotoma in controls do not reflect RP functional maps, indicating reorganization instead of adaptive processes

In order to understand if the remapping is a process of fast adaptation or chronic plasticity we decided to evaluate the retinotopic maps of the artificial scotoma control group. The-

oretically, if the maps of the controls of the AS group mimicked the RP maps, we would consider that the reorganization phenomena would reflect a process of fast adaptation.

After the pRF model estimation we noticed, qualitatively, that most of the estimated polar angle and eccentricity maps of the artificial scotoma group had very low signal-to-noise ratio (SNR). The few exceptions were cases AS4, whose maps are shown in Figure 3.1, whom mask effect was weaker (paired with RP4, with mean visual angle of 21.25 deg diameter) and cases AS8 and AS9 (RP mean visual fields covering 43 and 47.25 deg diameter, data not shown), with residual mask effects. Therefore, these two later cases had polar angle and eccentricity stimuli very similar to the original. The low SNR prevented the delineation of visual areas V1, V2 and V3 for the AS group.

By hypothesis, the mask overlaid included in the stimuli to simulate the visual field of a gender and age-matched patient with RP was not in fact representing the actual RP visual function, which led to incongruent representative maps between RP and AS cases. In other words, the AS maps do not replicate RP changes.

3.3.1 Analysis of Explained Variance along the occipital lobe

To understand the base of the lower SNR in AS group, we compared the performance of the pRFs modelling between all three groups. The quality of the model fit can be assessed through the values of the explained variance (R^2), which can be obtained by squaring each of the vertex's values of the given map R. We first performed a qualitative analysis of the graphs.

Firstly, we analysed the R^2 along the whole occipital lobe, since it is our region of interest, for all the participants of our three groups (Figure 3.14). There was a clear difference of R^2 between groups, which is higher in the Control group and lower in the AS group.

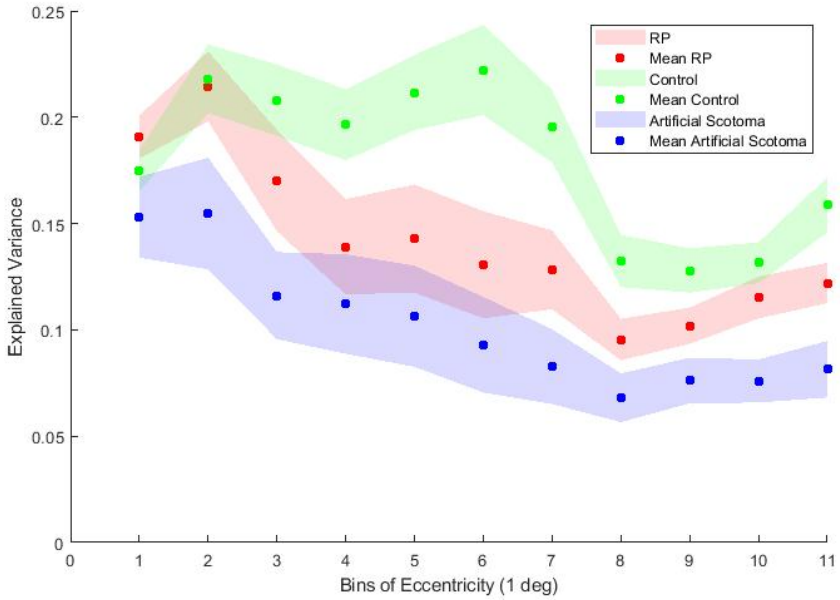

Figure 3.14: Representation of the mean explained variance R^2 for each eccentricity bin in the occipital lobe region for each group, RP (red), Control (green), Artificial Scotoma (blue). These results correspond to the mean of both hemispheres. The dots represent the mean R^2 value and the shadowed are the associated SEM.

After carefully inspecting the masks applied on each AS participant, we noticed that the individuals AS8 and AS9 could almost see the entire visual field, similarly to a control (see masks in Figure 2.1). As previously stated, AS8 and AS9 were paired to RP participants with mean visual fields spanning 43 and 47.25 deg diameter, respectively. This could mean these two could be influencing the results, because of representing a virtually unmasked situation and, therefore, we excluded them from the next analysis. Likewise, the matching RP patients (RP8 and RP9) were removed for the same reason and the calculation of the mean variance was redone (Figure 3.15). The difference between groups become even more evident.

The AS group values of R^2 decayed more evidently when we removed the patients with the masks who allowed them to *see more*. These result points out that bigger visual angle (larger visual field) would lead to a better model estimation. However, even RP patients with worse visual fields had higher R^2 values than their counterparts.

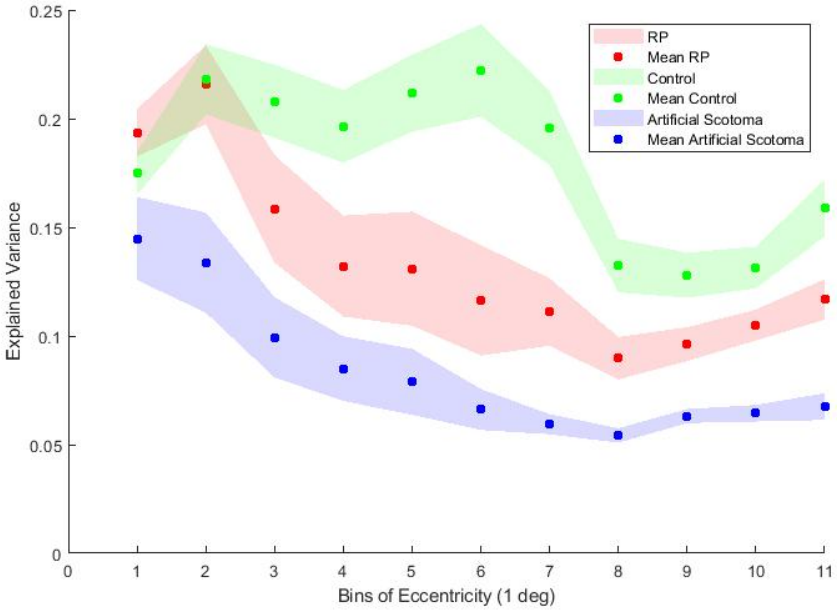

Figure 3.15: Representation of the mean variance R^2 for each eccentricity bin in the occipital lobe for each group, RP (red), Control (green), Artificial Scotoma (blue). RP8, RP9, AS8 and AS9 were removed from the analysis. These results correspond to the mean of both hemispheres. The dots represent the mean R^2 value and the shadowed area the associated SEM.

To confirm this claim, we subdivided the RP and the AS group into two subgroups according to the mean amount of visual angle *perceived* through the stimulated eye for each participant. Accordingly, four subgroups were analysed with a threshold of 15 deg (diameter) of visual angle (va): *RP, va* $\leqslant 15$ *deg* and *AS, va* $\leqslant 15$ *deg*, with mean visual angle lower or equal to 15 degrees of diameter, and *RP, va* > 15 *deg* and *AS, va* > 15 *deg*, with mean visual angle superior to 15 degrees. Then, we compared the mean explained variance R^2 along the eccentricity bins between controls, the two RP subgroups and the two AS subgroups (Figure 3.16).

This analysis shows that the division of the RP group and the AS group by an objective measure of the extent of what they *can see*, i.e. by their visual angle, leads to different model quality estimations. There is evidence that the less the participant sees, the worse the pRF model fitting. The worst fit (general lower R^2) is the AS group with visual angle inferior to 15 degrees, representing a person who is viewing a very small visual field through a mask. This means the mask in the artificial scotoma experiment is failing to

reproduce the RP visual function and also does not have enough power to produce good pRF fitting.

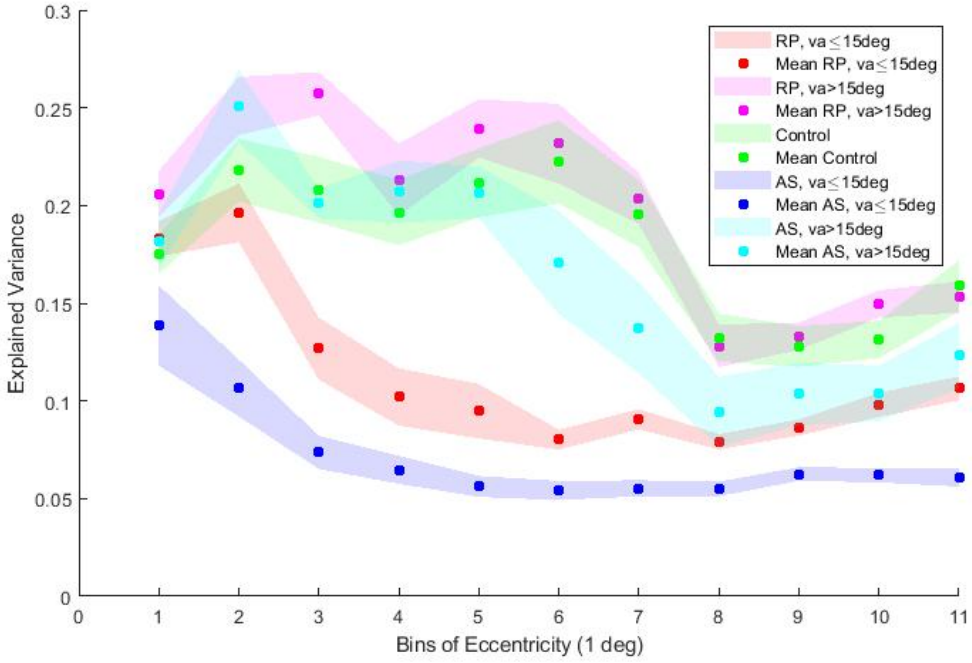

Figure 3.16: Representation of the mean variance R^2 for each eccentricity bin in the occipital lobe, for each group/subgoups, RP (RP, va⩽15deg, red and RP, va>15deg, pink), Control (green), Artificial Scotoma (AS, va⩽15deg dark blue and AS, va>15deg, light blue). These results corresponds to the mean of both hemispheres. The dots represent the mean R^2 value and the shadowed area the associated SEM.

Even if we can already conclude that R^2 is different between groups, the occipital lobe is a large region where anatomical definitions are problematic. For that reason, investigating the same variable on a smaller region could generate more reliable results.

3.3.2 Analysis of Explained Variance along the calcarine sulcus

Since visual areas V1, V2 and V3 are very hard to defined in the AS group, as already mentioned, we studied the explained variance R^2 along the calcarine sulcus. This region is located within V1 (anatomical division of ventral and dorsal V1) and can be manually drawn anatomically from the curvature maps. These maps were obtained from the anatomical reconstruction, in which all the sulci are represented. An example of the ex-

tent of the region considered for the calcarine sulcus is represented in Figure 3.17 for the left hemisphere.

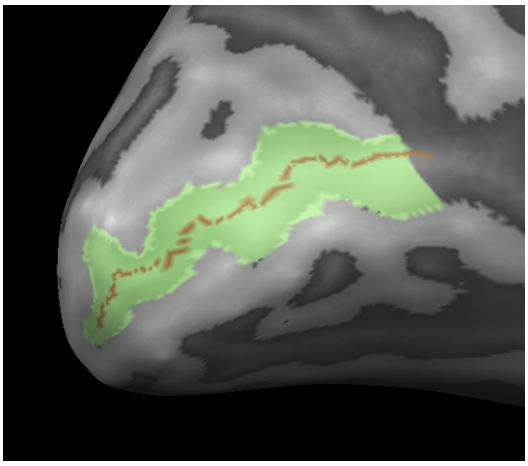

Figure 3.17: Manual delineation of the calcarine sulcus region (shadow in green) and the deepest part of it (represented as the brown line) on the left hemisphere.

Figure 3.18 represents the mean explained variance R^2 along each eccentricity bin of each group. As in the previous subsection (Subsection 3.3.1), in order to remove the effect of residual masks effects, patients RP8, RP9, and their respective control participants AS8 and AS9 were removed once again from the next analysis (Figure 3.19).

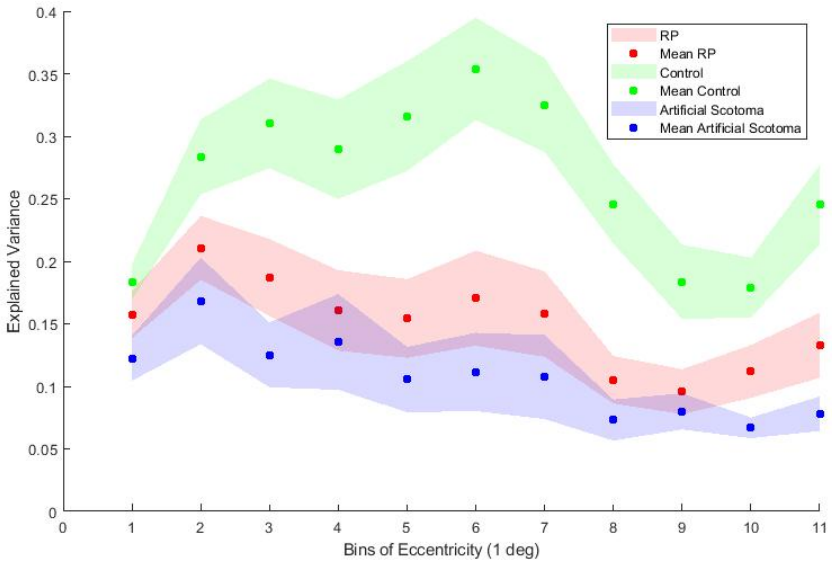

Figure 3.18: Representation of the mean explained variance R^2 for each eccentricity bin along the calcarine sulcus for each group, RP (red), Control (green), Artificial Scotoma (blue). These results correspond to the mean of both hemispheres. The dots represent the mean R^2 value and the shadowed area the associated SEM.

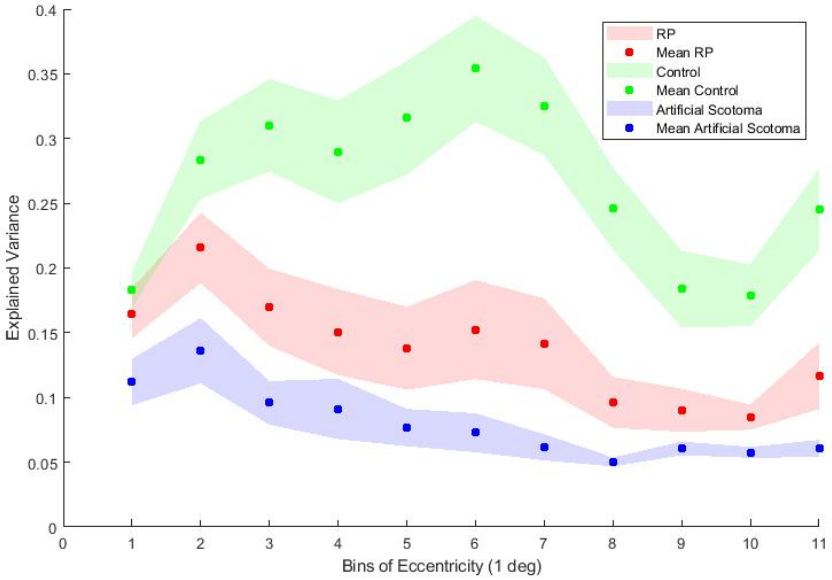

Figure 3.19: Representation of the mean explained variance R^2 for each eccentricity bin along the calcarine sulcus for each group, RP (red), Control (green), Artificial Scotoma (blue). These results correspond to the mean of both hemispheres. The dots represent the mean R^2 value and the shadowed area the associated SEM.

Afterwards, since we could not define early visual areas in the majority of participants of the AS group, and since the calcarine sulcus is a region encompassed by the primary visual field we analysed the mean size of the population receptive fields for each group on the calcarine sulcus (Figure 3.20).

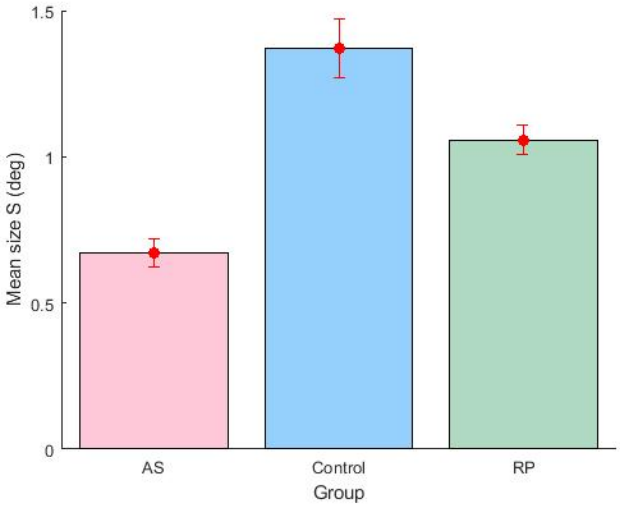

Figure 3.20: Illustration of the mean size of the whole calcarine sulcus for each group, along with the respective standard error. The outcome is the mean of both hemispheres.

The ANOVA for the mean pRF size as the independent variable revealed statistical differences between, at least, two groups ($F(2,34) = 24.63$, $p = 2.438 \times 10^{-7}$). A *post-hoc* testing revealed all groups had statistically different mean pRF sizes, i.e., RP and Control (RP-Control, $p = 0.010$), RP and AS (RP-AS, $p = 0.002$) as well as Control and AS (Control-AS, $p = 1.282 \times 10^{-7}$). Overall, Control group exhibited higher mean pRF sizes along the calcarine sulcus, and AS group the lowest values.

4

Discussion

Retinitis Pigmentosa (RP) is a rare inherited disease characterized by the degeneration of the photoreceptors. It leads to a progressive visual loss, that is predominant in the periphery, but eventually causes complete blindness [9, 42].

Functional and anatomical MRI data were acquired from twelve RP patients and thirty-five healthy controls (from which twelve participated in a artificial scotoma experiment (AS group) in order to study functional reorganization in RP patients). Despite the increasing number of reports aiming to study the visual plasticity phenomenon in several models of disease, this is still a very controversial topic. Moreover in RP, a model of genetically-determined peripheral loss of vision, this topic is even more poorly researched. The analysis consisted on the comparison of the population receptive fields sizes between the RP and the Control group, whose retinotopic maps (retinal topographies in the occipital cortex of the orderly representations of the visual field [48, 50]) were obtained using the improved technique named population receptive field (pRF) mapping. Additionally, in order to understand the origin of the remapping a paradigm with artificial scotoma patients was created and applied in healthy controls.

Generally, in healthy subjects a convergence of information exists throughout the visual system, which leads to an increase of the receptive field (RF) sizes with both eccentricity and along the visual pathway of the primate brain in general (Figure 4.1) [57].

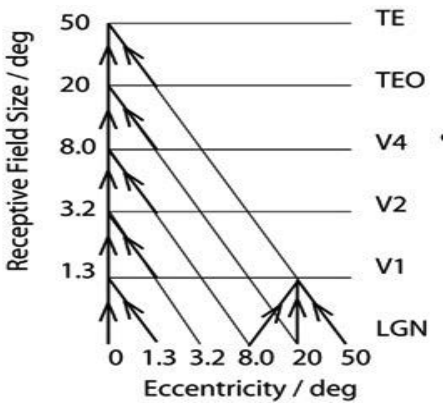

Figure 4.1: Representative model of convergence in the visual system of primates. LGN - lateral geniculate nucleus; V1 - primary visual area; TEO - posterior inferior temporal cortex; TE - inferior temporal cortex. Adapted from [58].

Dumoulin et al. (2008) also verified the enlargement of the population receptive field (pRF) sizes as a function of eccentricity measured in a range from 0 deg to 12 deg in healthy humans, reaching its maximum at the periphery. This expansion happens at successive processing stages in the visual pathway, which means is smaller in V1 and grows faster in V3 [51]. Similar outcome for the receptive fields within successive visual areas from V1 to V4, varying from 0deg to 12deg of eccentricity, have been obtained in monkeys using neurophysiological methods, with RFs in V1 being the smallest and the largest in V4 [59]. Our results from the data of the control group on the population receptive fields as a function of eccentricity reflect the process of convergence and are in agreement with the literature, corroborating the validity of this experiment.

On the other hand, data from the disease group RP suggests a loss of convergence between the visual areas, and within eccentricity, due to the fact that the degree of pRF sizes change along eccentricity bins and between visual areas is similar, in contrast with the control group. Furthermore, the visual inspection of mean pRFs of the two RP subgroups, divided according to the visual angle perceived, showed that this dissipation of the convergence of information might be linked to the magnitude of the visual field loss. However, possibly due to low statistical power, the differences have not been proven to be statistically significant.

V1 reorganization in patients with MD, whose disease leads to the degeneration of the central vision, has been linked to complete absence of bilateral foveal input [31]. An

evidence that could point to remapping in RP would be if there was an enlargement of the receptive field sizes in the peripheral part of V1 in order to compensate the lack of visual input, since the information is first received in the primary visual area and only afterwards conveys the visual information to V2 and V3 [16]. This is what is also found in animal models. In this study, we have found evidence that there is a change in the pRFs sizes in the periphery of V1 that is associated to the degree of visual area seen, since more narrow visual fields result in larger remapping (larger pRF sizes). This outcome is in line with a recent study from Ferreira et al. (2017), in which they have also suggested a topographic remapping in V1 of patients with RP. By measuring the distance between the most anterior point of each eccentricity ring (with a total of 8 rings) to the occipital pole for each participant, they found remapping that translated in a retinotopic shift of neuronal receptive fields in according to eccentricity and into regions with reduced retinal input (periphery, lesion projection zone). This shifting is, in addition, associated with the extent of visual field loss, with patients with less than 15 deg of available visual angle having a larger remapping [1], which is also in agreement with our experiment.

In order to understand the origin of the remapping previous studies have suggested the comparison of results between the disease group with another group with an artificial scotoma, mimicking their visual field extent [1, 38]. The artificial scotoma paradigm has been applied multiple times before while studying MD, a disease with central visual loss [29], and Baseler et al (2011), using retinotopy methods, concluded that the visual remapping is absent in MD [29]. This opens the question of the factors that determine whether reorganization is observed or not. Nonetheless, our research is the first to have an artificial scotoma (AS) paradigm, applied to healthy controls imitating patients with peripheral visual loss. We have found the lowest population receptive field sizes and the lowest explained variance, which defines the quality of the model fit, in the AS group. The observation that the maps in the AS group do not replicate the changes observed in RP suggests that 1) the remapping is not due to short-term adaptation but rather that is a result of long-term reorganization processes or 2) that artificial scotomas are not replicating the mechanisms associated with visual field loss by RP patients, namely that acquired filling-in strategies in RP may have been developed within the brain, i.e. the neural representations of the surroundings are being created instead of ignoring the absence of input in the scotoma

region [60]. In any case, the observed maps in RP do suggest that long-term changes in pRF properties are occurring. Hence, the visual field maps estimation is worst with lower extents of visual field. The conclusion from the artificial scotoma experiment is that, since the mask seem to not be mimicking RP visual fields, we can infer that the remapping in RP is not a fast adaptive process, i.e., it happens gradually over time. This seems to suggest the existence of plasticity in adults. However, more research should be made into finding a method of reversible visual loss that can actually simulate the real ones. A possible alternative would be transcraneal magnetic stimulation.

Previous studies that found reorganization in MD have been heavily criticized for the experimental design and their interpretation of the term *reorganization* [5], so more robust methods should be utilized, as for example pRF method with stimuli consisting of bars in different directions, which have been proven by Sendel et al. (2014) to be the most accurate in representing retinotopic maps [61]. This way it may be possible to achieve a consensus in the scientific community, which would lead to a progression in unveiling the phenomenon of visual plasticity and the treatment of the retinal diseases.

As in every experiment there were some limitations. While creating the artificial scotoma masks, the transition between central parts and the peripheral scotoma from the perimetric maps was considered as smoothed regions to prevent higher frequencies (and since it is a region of medium sensitivities) and therefore perceivable to a certain extent (shown as a light grey colour). Although this can be considered a limitation, the borders of a scotoma often have residual vision. When creating the stimulus time courses (.stm) file for the estimation of the pRFs, it is mandatory to use a binary version of the stimulus frames. The light grey region was defined as "*active*" and therefore as white, but can still be a source of error, since it was not a fully active region. The fact that some vision is still present in this region prevailed as a criterion. Moreover, due to the fact that visual areas are manually drawn over visual field maps, humans errors can occur on the definition of the ROIs boundaries for the pRF size analysis. Additionally, the fact that the stimulation was monocular, so we could apply perimetry masks on the original stimuli (AS group), reduced the SNR of the maps, which also constrained the ease of definition of the visual areas on all evaluated groups.

5

Conclusion

We have found strong evidence that supports functional reorganization on the visual cortex of individuals with Retinitis Pigmentosa (RP). This functional remapping was mirrored on the alterations of neuronal population receptive fields sizes in the peripheral eccentricities of the primary visual cortex (V1), that depend on the severity of visual field loss. The remapping is larger when the visual angles perceived by patients are smaller, i.e, at more advanced stages of the disease.

This study also lead to the assessment that the convergence of information in the visual cortex is gradually lost in these patients as a result of the degeneration of the visual field, i.e., smaller visual fields in higher level visual areas indicate a larger loss of convergence. This loss is reflected in the behavior of the receptive field sizes which do not grow along consecutive areas in the visual pathway, as expected. Although the growth still happens as a function of eccentricity, there is not a sharper increase in higher order visual areas.

Furthermore, the utilization of the artificial scotoma paradigm, in which controls would see a stimuli masked with the perimetric visual field of RP patients, contributed to dissect between short-term adaptation mechanisms or long-term reorganization. The explained variance was lower in this control experiment, which suggests lack of short-term reorganization when visual input deteriorates. Therefore, we may believe that the function remapping in RP is related to long-term plasticity processes.

Our study on receptive field reorganization and its independence from acute deterioration of visual input adds to the previous study by Ferreira et al. (2017) research and both imply that reorganization in adult patients with Retinitis Pigmentosa occurs weighted by

the progression of the disease, suggesting that the human brain does not fully loses his capability of plasticity even in adulthood.

6

Future Work

The indication that the human brain can reorganize itself even during adulthood to compensate for the damage produced by a certain event can open new doors to the development of new therapeutics to increase the patients' visual quality of life, like specific rehabilitation targetting the visually affected areas within each individual. However, future longitudinal studies still need to be made to understand the long-term effect of plasticity. It remains to be clarified whether the reorganization we have found is due to a good type of adaptation or a form of maladaptation, so new experiments are needed to fathom what specific phenomenon triggers the remapping and its functional consequences.

It would be of utmost interest to research on other diseases that lead to loss of peripheral vision, in order to figure out if the same effects can be observed. The analysis could be both in terms of population receptive field sizes and their migration within visual areas. The use of the population receptive field (pRF) technique is advised with the use of bars stimuli, instead of wedges and rings, presented randomly and with mean luminance periods, since it has been published to produce the best results for the estimation of the visual field maps [61].

Furthermore, in the literature it is recognized that ventral and dorsal pathways are dominated by central and periphery signals, respectively [12, 13]. Therefore, a study should be conducted where the dorsal and ventral parts of the visual areas are analysed separately, in order to discern the differences in terms of maintenance of convergence and the receptive field sizes within the periphery, if an actual difference exists between dorsal and ventral pathways.

Bibliography

[1] S. Ferreira, A. C. Pereira, B. Quendera, A. Reis, E. D. Silva, and M. Castelo-Branco, "Primary visual cortical remapping in patients with inherited peripheral retinal degeneration," *NeuroImage: Clinical*, vol. 13, pp. 428–438, 2017, doi: 10.1016/j.nicl.2016.12.013.

[2] E. Nava and B. Röder, "Adaptation and maladaptation," *Progress in Brain Research*, vol. 191, pp. 177–194, 2011, doi: 10.1016/B978-0-444-53752-2.00005-9.

[3] C. Gaser, G. Schlaug, G. Kempermann, H. G. Kuhn, J. Winkler, C. Büchel, and A. May, "Brain structures differ between musicians and non-musicians." *The Journal of neuroscience : the official journal of the Society for Neuroscience*, vol. 23, no. 27, pp. 9240–5, oct 2003, doi: 10.1523/jneurosci.4628-05.2006.

[4] G. Denes, *Neural plasticity across the lifespan : how the brain can change*. Psychology Press, 2015, ISBN: 1317909941, Accessed on: 2019-04-04.

[5] J. Lemos, D. Pereira, and M. Castelo-Branco, "Visual Cortex Plasticity Following Peripheral Damage To The Visual System: fMRI Evidence," *Current Neurology and Neuroscience Reports*, vol. 16, no. 10, p. 89, oct 2016, doi: 10.1007/s11910-016-0691-0.

[6] B. A. Wandell and S. M. Smirnakis, "Plasticity and stability of visual field maps in adult primary visual cortex," *Nature Reviews Neuroscience*, vol. 10, no. 12, pp. 873–884, 2009, doi: 10.1038/nrn2741.

[7] B. Kolb and I. Q. Whishaw, "What Are the Origins of Brain and Behavior?" *Human Evolution*, pp. 1–16, 2005, Accessed on: 2019-04-04. [Online]. Available: https:

//www.ndsu.edu/faculty/pavek/Psych486_686/chapterpdfs1stedKolb/Kolb_01.pdf

[8] C. D. Gilbert and W. Li, "Adult Visual Cortical Plasticity," *Neuron*, vol. 75, no. 2, pp. 250–264, 2012, doi: 10.1016/j.neuron.2012.06.030.

[9] K. J. Wert, J. H. Lin, and S. H. Tsang, "General pathophysiology in retinal degeneration," *Cell-Based Therapy for Retinal Degenerative Disease*, vol. 53, pp. 33–43, 2014, doi: 10.1159/000357294.

[10] P. E. Ludwig and C. N. Czyz, *Physiology, Eye*. StatPearls Publishing, feb 2019, Accessed on: 2019-05-25. [Online]. Available: http://www.ncbi.nlm.nih.gov/pubmed/29262001

[11] B. Laha, B. K. Stafford, and A. D. Huberman, "Regenerating optic pathways from the eye to the brain," *Science*, vol. 356, no. 6342, pp. 1031–1034, 2017, doi: 10.1126/science.aal5060.

[12] L. G. Ungerleider and R. Desimone, "Projections to the superior temporal sulcus from the central and peripheral field representations of V1 and V2," *Journal of Comparative Neurology*, vol. 248, no. 2, pp. 147–163, 1986, doi: 10.1002/cne.902480202.

[13] R. Gattass, S. Nascimento-Silva, J. G. M. Soares, B. Lima, A. K. Jansen, A. C. M. Diogo, M. F. Farias, M. M. E. P. Botelho, O. S. Mariani, J. Azzi, M. Fiorani, and M. Fiorani, "Cortical visual areas in monkeys: location, topography, connections, columns, plasticity and cortical dynamics." *Philosophical transactions of the Royal Society of London. Series B, Biological sciences*, vol. 360, no. 1456, pp. 709–31, apr 2005, doi: 10.1098/rstb.2005.1629.

[14] N. Sanda, L. Cerliani, C. N. Authié, N. Sabbah, J.-A. Sahel, C. Habas, A. B. Safran, and M. Thiebaut de Schotten, "Visual brain plasticity induced by central and peripheral visual field loss," *Brain Structure and Function*, vol. 223, no. 7, pp. 3473–3485, sep 2018, doi: 10.1007/s00429-018-1700-7.

[15] "Photoreceptors - American Academy of Ophthalmology," 2017, Accessed on: 2019-05-25. [Online]. Avail-

able: https://www.aao.org/eye-health/anatomy/photoreceptors?fbclid=IwAR1oJnLw{_}946LqSxjCThhrQSfa4giKcQdxT7LF9rav{_}-H7mWMtI9Iyx4avg

[16] T. Huff and P. Tadi, *Neuroanatomy, Visual Cortex*. StatPearls Publishing, mar 2019, Accessed on: 2019-06-22. [Online]. Available: http://www.ncbi.nlm.nih.gov/pubmed/29494110

[17] Miquel Perello Nieto, "File:Human visual pathway.svg - Wikipedia," 2015, Accessed on: 2019-05-26. [Online]. Available: https://en.wikipedia.org/wiki/File:Human{_}visual{_}pathway.svg

[18] O. C. D'Almeida, C. Mateus, A. Reis, M. M. Grazina, and M. Castelo-Branco, "Long term cortical plasticity in visual retinotopic areas in humans with silent retinal ganglion cell loss," *NeuroImage*, vol. 81, pp. 222–230, 2013, doi: 10.1016/j.neuroimage.2013.05.032.

[19] J. Kaas, L. Krubitzer, Y. Chino, A. Langston, E. Polley, and N. Blair, "Reorganization of retinotopic cortical maps in adult mammals after lesions of the retina," *Science*, vol. 248, no. 4952, pp. 229–231, apr 1990, doi: 10.1126/science.2326637.

[20] Y. M. Chino, J. H. Kaas, E. L. Smith, A. L. Langston, and H. Cheng, "Rapid reorganization of cortical maps in adult cats following restricted deafferentation in retina," *Vision Research*, vol. 32, no. 5, pp. 789–796, 1992, doi: 10.1016/0042-6989(92)90021-A.

[21] C. Darian-Smith and C. D. Gilbert, "Topographic reorganization in the striate cortex of the adult cat and monkey is cortically mediated." *The Journal of neuroscience : the official journal of the Society for Neuroscience*, vol. 15, no. 3 Pt 1, pp. 1631–47, mar 1995, doi: 10.1523/JNEUROSCI.15-03-01631.1995.

[22] T. Keck, T. D. Mrsic-Flogel, M. Vaz Afonso, U. T. Eysel, T. Bonhoeffer, and M. Hübener, "Massive restructuring of neuronal circuits during functional reorganization of adult visual cortex," *Nature Neuroscience*, vol. 11, no. 10, pp. 1162–1167, 2008, doi: 10.1038/nn.2181.

[23] E. P. Botelho, C. Ceriatte, J. G. Soares, R. Gattass, and M. Fiorani, “Quantification of Early Stages of Cortical Reorganization of the Topographic Map of V1 Following Retinal Lesions in Monkeys,” *Cerebral Cortex (New York, NY)*, vol. 24, no. 1, p. 1, jan 2014, doi: 10.1093/CERCOR/BHS208.

[24] I. Murakami, H. Komatsu, and M. Kinoshita, “Perceptual filling-in at the scotoma following a monocular retinal lesion in the monkey,” *Visual Neuroscience*, vol. 14, no. 1, pp. 89–101, 1997, doi: 10.1017/s0952523800008798.

[25] S. M. Smirnakis, A. A. Brewer, M. C. Schmid, A. S. Tolias, A. Schüz, M. Augath, W. Inhoffen, B. A. Wandell, and N. K. Logothetis, “Lack of long-term cortical reorganization after macaque retinal lesions,” *Nature*, vol. 435, no. 7040, pp. 300–307, 2005, doi: 10.1038/nature03495.

[26] H. A. Baseler, A. A. Brewer, L. T. Sharpe, A. B. Morland, H. Jägle, and B. A. Wandell, “Reorganization of human cortical maps caused by inherited photoreceptor abnormalities,” *Nature Neuroscience*, vol. 5, no. 4, pp. 364–370, apr 2002, doi: 10.1038/nn817.

[27] J. S. Sunness, T. Liu, and S. Yantis, “Retinotopic mapping of the visual cortex using functional magnetic resonance imaging in a patient with central scotomas from atrophic macular degeneration,” *Ophthalmology*, vol. 111, no. 8, pp. 1595–1598, aug 2004, doi: 10.1016/j.ophtha.2003.12.050.

[28] Y. Masuda, S. O. Dumoulin, S. Nakadomari, and B. A. Wandell, “V1 projection zone signals in human macular degeneration depend on task, not stimulus.” *Cerebral cortex (New York, N.Y. : 1991)*, vol. 18, no. 11, pp. 2483–93, nov 2008, doi: 10.1093/cercor/bhm256.

[29] H. A. Baseler, A. Gouws, K. V. Haak, C. Racey, M. D. Crossland, A. Tufail, G. S. Rubin, F. W. Cornelissen, and A. B. Morland, “Large-scale remapping of visual cortex is absent in adult humans with macular degeneration,” *Nature Neuroscience*, vol. 14, no. 5, pp. 649–655, may 2011, doi: 10.1038/nn.2793.

[30] C. I. Baker, E. Peli, N. Knouf, and N. G. Kanwisher, “Reorganization of Visual Processing in Macular Degeneration,” *Journal of Neuroscience*, vol. 25, no. 3, pp.

614–618, jan 2005, doi: 10.1523/JNEUROSCI.3476-04.2005.

[31] C. I. Baker, D. D. Dilks, E. Peli, and N. Kanwisher, “Reorganization of visual processing in macular degeneration: replication and clues about the role of foveal loss.” *Vision research*, vol. 48, no. 18, pp. 1910–9, aug 2008, doi: 10.1016/j.visres.2008.05.020.

[32] D. D. Dilks, J. B. Julian, E. Peli, and N. Kanwisher, “Reorganization of Visual Processing in Age-Related Macular Degeneration Depends on Foveal Loss,” *Optometry and Vision Science*, vol. 91, no. 8, pp. e199–e206, aug 2014, doi: 10.1097/OPX.0000000000000325.

[33] E. H. Schumacher, J. A. Jacko, S. A. Primo, K. L. Main, K. P. Moloney, E. N. Kinzel, and J. Ginn, “Reorganization of visual processing is related to eccentric viewing in patients with macular degeneration.” *Restorative neurology and neuroscience*, vol. 26, no. 4-5, pp. 391–402, 2008. [Online]. Available: http://www.ncbi.nlm.nih.gov/pubmed/18997314

[34] T. Liu, S.-H. Cheung, R. A. Schuchard, C. B. Glielmi, X. Hu, S. He, and G. E. Legge, “Incomplete cortical reorganization in macular degeneration.” *Investigative ophthalmology & visual science*, vol. 51, no. 12, pp. 6826–34, dec 2010, doi: 10.1167/iovs.09-4926.

[35] D. D. Dilks, C. I. Baker, E. Peli, and N. Kanwisher, “Reorganization of visual processing in macular degeneration is not specific to the ”preferred retinal locus”.” *The Journal of neuroscience : the official journal of the Society for Neuroscience*, vol. 29, no. 9, pp. 2768–73, mar 2009, doi: 10.1523/JNEUROSCI.5258-08.2009.

[36] V. M. Borges, H. V. Danesh-Meyer, J. M. Black, and B. Thompson, “Functional effects of unilateral open-angle glaucoma on the primary and extrastriate visual cortex,” *Journal of Vision*, vol. 15, no. 15, p. 9, nov 2015, doi: 10.1167/15.15.9.

[37] W. Zhou, E. R. Muir, K. S. Nagi, S. Chalfin, P. Rodriguez, and T. Q. Duong, “Retinotopic fMRI Reveals Visual Dysfunction and Functional Reorganization in the Visual Cortex of Mild to Moderate Glaucoma Patients,” *Journal of Glaucoma*, vol. 26, no. 5, pp. 430–437, may 2017, doi: 10.1097/IJG.0000000000000641.

[38] Y. Masuda, H. Horiguchi, S. O. Dumoulin, A. Furuta, S. Miyauchi, S. Nakadomari, and B. A. Wandell, "Task-Dependent V1 Responses in Human Retinitis Pigmentosa," *Investigative Ophthalmology & Visual Science*, vol. 51, no. 10, p. 5356, 2010, doi: 10.1167/IOVS.09-4775.

[39] S. Ferreira, A. C. Pereira, B. Quendera, A. Reis, E. D. Silva, and M. Castelo-Branco, "Enhanced Visual Attentional Modulation in Patients with Inherited Peripheral Retinal Degeneration in the Absence of Cortical Degeneration," *Neural Plasticity*, vol. 2019, pp. 1–14, jun 2019, doi: 10.1155/2019/8136354.

[40] A. Martins Rosa, M. F. Silva, S. Ferreira, J. Murta, and M. Castelo-Branco, "Plasticity in the human visual cortex: an ophthalmology-based perspective." *BioMed research international*, vol. 2013, p. 568354, sep 2013, doi: 10.1155/2013/568354.

[41] P. Mateos-aparicio and A. Rodríguez-moreno, "The Impact of Studying Brain Plasticity," *Front. Cell. Neurosci.*, vol. 13, no. February, pp. 1–5, 2019, doi: 10.3389/fncel.2019.00066.

[42] S. Ferrari, E. Di Iorio, V. Barbaro, D. Ponzin, F. S. Sorrentino, and F. Parmeggiani, "Retinitis pigmentosa: genes and disease mechanisms." *Current genomics*, vol. 12, no. 4, pp. 238–49, jun 2011, doi: 10.2174/138920211795860107.

[43] S. P. Daiger, L. S. Sullivan, and S. J. Bowne, "Genes and mutations causing retinitis pigmentosa." *Clinical genetics*, vol. 84, no. 2, pp. 132–41, aug 2013, doi: 10.1111/cge.12203.

[44] C. Hamel, "Retinitis pigmentosa." *Orphanet journal of rare diseases*, vol. 1, p. 40, oct 2006, doi: 10.1186/1750-1172-1-40.

[45] G. R. Fink, "Functional Magnetic Resonance Imaging," *Neurobiology of Disease*, pp. 839–848, jan 2007, doi: 10.1016/B978-012088592-3/50079-7.

[46] P. M. Matthews and P. Jezzard, "Functional magnetic resonance imaging." *Journal of neurology, neurosurgery, and psychiatry*, vol. 75, no. 1, pp. 6–12, jan 2004. [Online]. Available: http://www.ncbi.nlm.nih.gov/pubmed/14707297

[47] K. Nimmagadda and J. D. Weiland, "Retinotopic Responses in the Visual Cortex Elicited by Epiretinal Electrical Stimulation in Normal and Retinal Degenerate Rats," *Translational Vision Science & Technology*, vol. 7, no. 5, p. 33, oct 2018, doi: 10.1167/tvst.7.5.33.

[48] L. Henriksson, J. Karvonen, N. Salminen-Vaparanta, H. Railo, and S. Vanni, "Retinotopic maps, spatial tuning, and locations of human visual areas in surface coordinates characterized with multifocal and blocked FMRI designs." *PloS one*, vol. 7, no. 5, p. e36859, 2012, doi: 10.1371/journal.pone.0036859.

[49] B. R. White and J. P. Culver, "NeuroImage Phase-encoded retinotopy as an evaluation of diffuse optical neuroimaging," *NeuroImage*, vol. 49, no. 1, pp. 568–577, 2010, doi: 10.1016/j.neuroimage.2009.07.023.

[50] J. Warnking, M. Dojat, A. Gue, N. Richard, A. Che, and C. Segebarth, "fMRI Retinotopic Mapping — Step by Step," *NeuroImage*, vol. 1683, pp. 1665–1683, 2002, doi: 10.1006/nimg.2002.1304.

[51] S. O. Dumoulin and B. A. Wandell, "Population receptive field estimates in human visual cortex," *NeuroImage*, vol. 39, no. 2, pp. 647–660, 2008, doi: 10.1016/j.neuroimage.2007.09.034.

[52] J. D. Victor, K. Purpura, E. Katz, and B. Mao, "Population encoding of spatial frequency, orientation, and color in macaque V1." *Journal of neurophysiology*, vol. 72, no. 5, pp. 2151–66, nov 1994, doi: 10.1152/jn.1994.72.5.2151.

[53] S. O. Dumoulin, K. Amano, and B. A. Wandell, "Quantitative population receptive field estimates in human visual cortex," *Journal of Vision*, vol. 8, no. 17, pp. 35–35, mar 2010, doi: 10.1167/8.17.35.

[54] "BrainVoyager QX User's Guide," http://www.brainvoyager.com/bvqx/doc/UsersGuide/BrainVoyagerQXUsersGuide.html, Accessed on: 2019-04-02.

[55] Y. Lee, "What repeated measures analysis of variances really tells us." *Korean journal of anesthesiology*, vol. 68, no. 4, pp. 340–5, aug 2015, doi: 10.4097/kjae.2015.68.4.340.

[56] L. E. Welbourne, A. B. Morland, and A. R. Wade, "Population receptive field (pRF) measurements of chromatic responses in human visual cortex using fMRI." *NeuroImage*, vol. 167, pp. 84–94, 2018, doi: 10.1016/j.neuroimage.2017.11.022.

[57] M. Carrasco and A. Barbot, "How Attention Affects Spatial Resolution." *Cold Spring Harbor symposia on quantitative biology*, vol. 79, pp. 149–60, 2014, doi: 10.1101/sqb.2014.79.024687.

[58] E. T. Rolls, "Invariant Visual Object and Face Recognition: Neural and Computational Bases, and a Model, VisNet," *Frontiers in Computational Neuroscience*, vol. 6, p. 35, jun 2012, doi: 10.3389/fncom.2012.00035.

[59] A. Smith, K. Singh, A. Williams, and M. Greenlee, "Estimating Receptive Field Size from fMRI Data in Human Striate and Extrastriate Visual Cortex," *Cerebral Cortex*, vol. 11, no. 12, pp. 1182–1190, dec 2001, doi: 10.1093/cercor/11.12.1182.

[60] V. S. Ramachandran and R. L. Gregory, "Perceptual filling in of artificially induced scotomas in human vision," *Nature*, vol. 350, no. 6320, pp. 699–702, apr 1991, doi: 10.1038/350699a0.

[61] M. Senden, J. Reithler, S. Gijsen, and R. Goebel, "Evaluating Population Receptive Field Estimation Frameworks in Terms of Robustness and Reproducibility," *PLoS ONE*, vol. 9, no. 12, p. e114054, dec 2014, doi: 10.1371/journal.pone.0114054.

Appendices

Appendix A

Table 6.1: Neuro-ophtalmologic characteristics of the participants' sample. Average Retinal and Retinal Nerve Fiber Layer (RNFL) thickness were measured using frequency domain Cirrus Ocular Coherence Tomography (OCT, software version 5.1.1.6, Carl Zeiss Meditec AG, USA). Moreover, it was used a suprathreshold strategy for the 79 visual field points tested in central 24 deg, or 12 deg when patients had a small visual field, to automatically obtain the visual field deficit volume based on sensitivity values of those points and tested visual area.

ID	Group	Mean Retina Thickness (µm)	Mean RNFL Thickness (µm)	Mean Deficit Volume (dB)	Visual Field Device
RP1	RP	226,5	102,5	20,85	Metrovision Fast-24
RP2	RP	201	108	22,8	Metrovision Fast-24
RP3	RP	235,5	90	21,95	Metrovision Fast-24
RP4	RP	253,5	128	17,1	Metrovision Fast-24
RP5	RP (USH)	217	105,5	22,1	Metrovision Fast-24
RP6	RP	273	101	20,2	Metrovision Fast-24
RP7	RP	260	136,5	16,95	Metrovision Fast-12
RP8	RP	243,5	98	7,25	Metrovision Fast-24
RP9	RP	270,5	91,5	1,35	Metrovision Fast-24
RP10	RP (USH)	216,5	96	20,2	Metrovision Fast-24
RP11	RP (USH)	252	127	16,8	Metrovision Fast-12
RP12	RP (USH)	219,5	100	21,6	Metrovision Fast-24
CNTR1	Control	282	83	0,65	Metrovision Fast-24
CNTR2	Control	308	108,5	0,3	Metrovision Fast-24
CNTR3	Control	294	98,5	0,5	Metrovision Fast-24
CNTR4	Control	257,5	78	0,3	Metrovision Fast-24
CNTR5	Control	275	83	-0,3	Octopus
CNTR6	Control	278	95,5	0,1	Metrovision Fast-24
CNTR7	Control	277	99	0	Metrovision Fast-24
CNTR8	Control	279,5	88,5	0,3	Metrovision Fast-24
CNTR9	Control	303	107,5	0,05	Metrovision Fast-24
CNTR10	Control	279,5	92	0,35	Metrovision Fast-24
CNTR11	Control	304	113	0	Metrovision Fast-24
CNTR12	Control	294	98,5	0,2	Metrovision Fast-24
CNTR13	Control	280,5	94	-0,95	Octopus
AS1	Control Simulated	288,5	90,5	0,15	Octopus
AS2	Control Simulated	283	118	0,4	Metrovision Fast-24
AS3	Control Simulated	275	95	-1,2	Octopus
AS4	Control Simulated	285	99,5	1,45	Octopus
AS5	Control Simulated	275	108	0,2	Metrovision Fast-24
AS6	Control Simulated	296,5	101,5	0,1	Metrovision Fast-24
AS7	Control Simulated	284	93	0,3	Metrovision Fast-24
AS8	Control Simulated	280,5	100	1,9	Octopus
AS9	Control Simulated	292	81	1,95	Octopus
AS10	Control Simulated	281,5	80,5	0,3	Metrovision Fast-24
AS11	Control Simulated	286	85,5	0,75	Metrovision Fast-24
AS12	Control Simulated	300	93	-0,35	Octopus

Appendix B

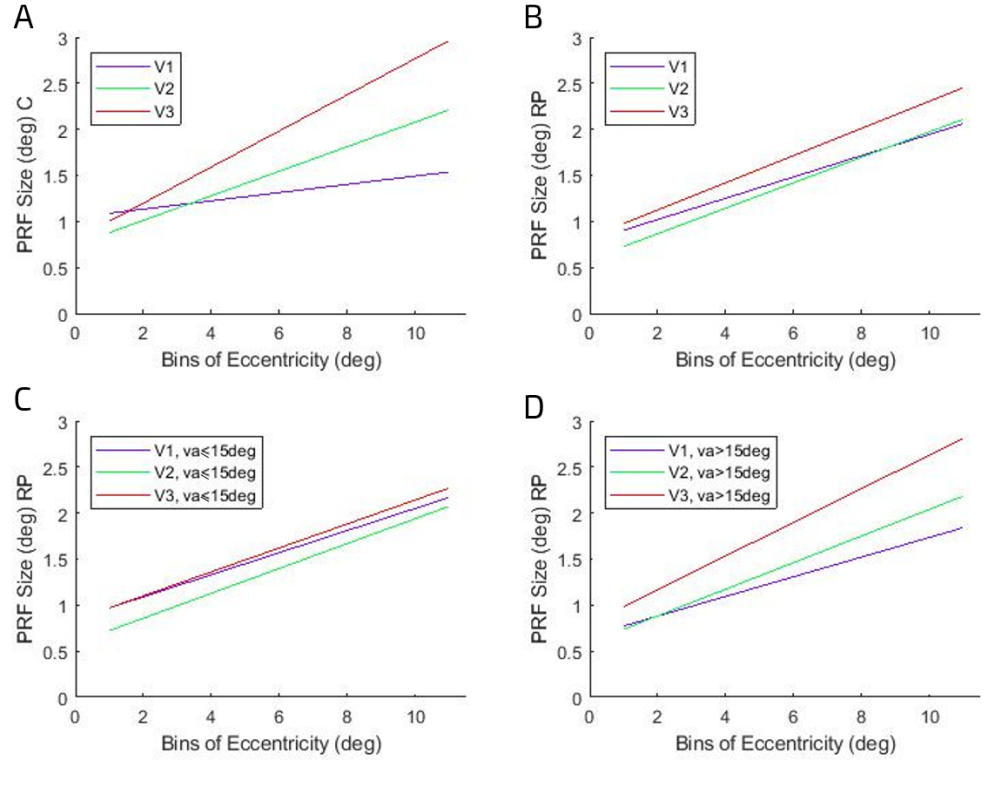

Figure 6.1: Data representation of the mean population receptive field sizes in function of eccentricity within visual areas V1, V2 and V3 of all the participants from (A) the control group and (B) the RP group. (C) and (D) represent the same analysis but for RP subgroup with visual angle (va) smaller or equal to 15 degrees (*RP, va* $\leqslant 15$ *deg*) and RP subgroup whose patients had visual angles superior to 15 degrees (*RP, va*> 15 *deg*), respectively.